High-Order Accurate Time-Stepping Schemes for Convection-Diffusion Problems

J. Donea
B. Roig
A. Huerta

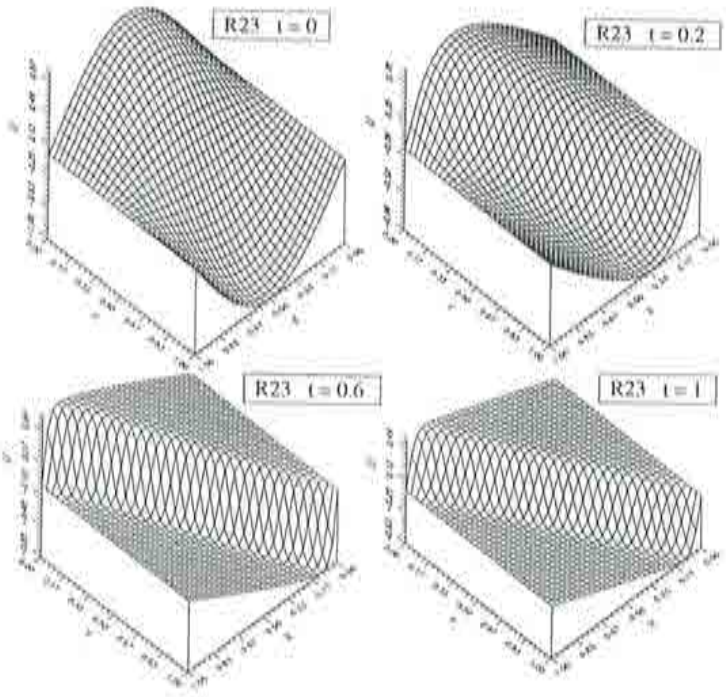

Monograph CIMNE Nº 42, July 1998

High-Order Accurate Time-Stepping Schemes for Convection-Diffusion Problems

J. Donea
LTAS, Institute of Mechanics, University of Liège
21 rue E. Solvay, B-4000 Liège, Belgium

B. Roig and A. Huerta
Universitat Politècnica de Catalunya
Dpto. Matemàtica Aplicada III
E-08034 Barcelona, Spain

Monograph CIMNE Nº 42, July 1998

International Center for Numerical Methods in Engineering
Gran Capitán s/n, 08034 Barcelona, Spain

The cover designed by: Jordi Palli

First published, July 1998

Edited by:
International Center for Numerical Methods in Engineering
C/ Gran Capitán, s/n
08034 Barcelona, Spain

ISBN: 84-89925-24-0
Deposito Legal: B-37870-98

Contents

1 Introduction

In an attempt to develop efficient finite element schemes for the numerical simulation of time-dependent convective transport problems, Taylor-Galerkin (TG) schemes with third- and fourth-order accuracy in the time step were developed over the last years and successfully applied in the solution of engineering problems. See for instance references [3, 5, 6] for an overview of the properties of third and fourth order TG schemes for pure advection. Practical applications of TG methods in the solution of linear and nonlinear convective transport problems are described in references [7, 18, 26].

By contrast, the application of higher-order TG schemes to mixed problems describing transient transport by both convection and diffusion appears to be much more difficult. This is due to the presence of the Laplacian operator in the governing equation which does not allow the TG procedure to be carried out to third or higher order in conjunction with the use of standard C^0 finite elements for spatial discretization. Reference [4] presents an early study of second-order Taylor-Galerkin schemes for convection-diffusion problems.

In the present paper, a study has been made of other high order time-stepping methods with the view of identifying schemes that could possibly be used for a time accurate finite element solution of transient problems describing convective-diffusive transport. Both explicit and implicit methods are considered.

To be easily implemented, higher-order time-stepping schemes for the convection-diffusion equation should not involve higher-order time derivatives. This is the case for Runge-Kutta methods [8, 9] , as well as for multi-stage schemes emanating from Padé approximations to the exponential function [1, 17, 21]. As will be shown, these methods achieve higher-order accuracy through a multi-stage process involving first time derivatives only. Moreover, some implicit methods possess the interesting property of unconditional stability in application to hybrid parabolic-hyperbolic equations. They should thus prove useful for solving transient advection-diffusion problems using finite elements.

To provide a starting point for the subsequent developments, we recall in Section 2 the basic steps leading to second order accurate TG schemes for the linear advection-diffusion equation.

Ways to improve the accuracy of such TG schemes in the presence of convection dominated situations are discussed in Section 3.

This is followed in Section 4 by a discussion of multi-stage schemes obtained from Padé approximations to the exponential function. The properties of such schemes are analyzed in detail in Section 5 including their stability domain in 1D and 2D, and their phase and damping responses.

Then, Runge-Kutta methods of high order are introduced in Section 6. Both explicit and implicit methods are considered. Their properties are compared with those of corresponding Padé approximations.

Other higher-order implicit methods are analyzed in Section 7 where implicit schemes of second, fourth and sixth order accuracy are derived through Simpson's

quadrature rule. To this end, a given polynomial representation of the first time derivative is assumed over a typical time step.
While the computer implementation of the explicit time-stepping methods does not pose any problem, the situation is quite different when high order implicit methods are used. In fact, such methods generate sets of coupled first-order equations which give rise to large algebraic systems of unsymmetric and possibly nonlinear equations.
Numerical results are then presented in Section 8 to confirm the accuracy and stablility properties of some of the multistage methods considered in the paper. In particular, a new two dimensional Burgers test problem with analytical solution is presented.
Finally, Section 9 presents the main conclusions of the present study and indicates the lines of further research developements in the area of convection-diffusion phenomena.

2 Basic second order TG scheme

In order to introduce the second order TG method for evolutionary advection-diffusion problems in the simplest possible way, while retaining all the essential features of the method, we first consider the linear advection-diffusion equation for the scalar quantity u

$$u_t = -\boldsymbol{a} \cdot \nabla u + \nu \nabla^2 u, \tag{1}$$

where $\boldsymbol{a}$ is the advection velocity and $\nu > 0$ the diffusion coefficient. Both $\boldsymbol{a}$ and ν are assumed to be constant.
By contrast with the current practice in the finite element solution of initial boundary value problems which consists of performing spatial discretization before time discretization, the reverse is true in the TG approach. In fact, like in the Lax-Wendroff finite difference method, time discretization preceeds space discretization in the TG approach.

2.1 Time discretization

Let us thus leave the spatial variables $\boldsymbol{x}$ continuous and discretize Eq.(1) in time with the aid of the following Taylor series expansion

$$(u^{n+1} - u^n)/\Delta t = u_t^n + \frac{1}{2}\Delta t\, u_{tt}^n + O(\Delta t^2) \tag{2}$$

which includes first- and second-order time derivatives. While the former is provided directly by Eq.(1), the latter can be obtained by taking the time derivative of the governing partial differential equation (1) which gives

$$u_{tt} = -\boldsymbol{a} \cdot \nabla u_t + \nu\, \nabla^2 u_t. \tag{3}$$

At this point we note that the right-hand side of (3) has to be left in its mixed spatial-temporal form, because the elimination of u_t through (1) would introduce higher-order spatial derivatives which would preclude the use of finite elements with C^0 continuity (e.g. the Lagrange family) for the spatial discretization. For the same reason the Taylor series expansion (2) had to be limited to the second-order time derivative. This is in contrast with the pure advection case ($\nu = 0$) for which the third-order time derivative can be retained in the Taylor series and schemes devised with third-order accuracy in the time step (see [3]).
The substitution of u_t^n and u_{tt}^n in Taylor expansion (2) yields the semi-discrete equation

$$(u^{n+1} - u^n)/\Delta t = (-\boldsymbol{a}\cdot\boldsymbol{\nabla} + \nu\nabla^2)u^n + \frac{1}{2}\Delta t(-\boldsymbol{a}\cdot\boldsymbol{\nabla} + \nu\nabla^2)u_t^n \qquad (4)$$

which, upon approximation of u_t^n by $(u^{n+1} - u^n)/\Delta t$, can be rearranged as

$$[1 - \frac{1}{2}\Delta t(-\boldsymbol{a}\cdot\boldsymbol{\nabla} + \nu\nabla^2)]\,(u^{n+1} - u^n)/\Delta t = (-\boldsymbol{a}\cdot\boldsymbol{\nabla} + \nu\nabla^2)\,u^n. \qquad (5)$$

Scheme (5) is, by construction, second-order accurate in the time step and it is immediate to recognize that it represents an incremental form of the Crank-Nicolson time-stepping method. This is, however, not the case when variable coefficient or nonlinear equations are considered.

2.2 Spatial discretization

To obtain a fully discrete equation, we apply the Galerkin formulation to scheme (5) with local approximations of the form

$$U^n(x) = \sum_I N_I(x)\,U_I^n. \qquad (6)$$

Introducing the incremental unknown $W^{n+1} = U^{n+1} - U^n$, and denoting by $\langle u\,,\,w\rangle$ the L_2 inner product $\int_\Omega u\,w\,d\Omega$ over the domain of the problem, and $\langle u\,,\,w\rangle_\Gamma$ the L_2 product $\int_\Gamma u\,w\,d\Gamma$ over the contour of the domain, the Galerkin equations take the form

$$\begin{aligned} \langle W^{n+1}\,,\,N_I\rangle/\Delta t + \frac{1}{2}\langle \boldsymbol{a}\cdot\boldsymbol{\nabla}W^{n+1}\,,\,N_I\rangle \;+\; & \frac{1}{2}\langle \nu\,\boldsymbol{\nabla}W^{n+1}\,,\,\boldsymbol{\nabla}N_I\rangle \\ -\frac{1}{2}\left\langle \nu\,\boldsymbol{n}\cdot\boldsymbol{\nabla}W^{n+1},\,N_I\right\rangle_\Gamma \;=\; & -\langle \boldsymbol{a}\cdot\boldsymbol{\nabla}U^n\,,\,N_I\rangle \\ -\langle \nu\,\boldsymbol{\nabla}U^n\,,\,\boldsymbol{\nabla}N_I\rangle \;+\; & \langle \nu\,\boldsymbol{n}\cdot\boldsymbol{\nabla}U^n,\,N_I\rangle_\Gamma \qquad \forall\, I. \end{aligned} \qquad (7)$$

Equation (7) is valid for arbitrary basis functions N_I and form the basis for developing Taylor-Galerkin finite element schemes for the advection-diffusion equation (1). At this point, it is important to note that the unknown W^{n+1} is governed by an unsymmetric generalized mass matrix. This is indeed due to

the presence of the unsymmetric convection operator. Moreover, since the mass matrix includes all the additional terms due to the second-order accuracy in time, the TG procedure is clearly ineffective for transient problems evolving towards a highly convective steady state. This difficulty may be circumvented by the use of a splitting-up method in which the advection-diffusion problem is decomposed into a pure advection problem followed by a pure diffusion one [4]. This kind of schemes usually have a low order precision.

2.3 Application to linear basis functions

In the case of piecewise linear basis functions on a uniform 1D mesh of size h, Eq.(7) can be written in terms of the nodal parameters U_j^n as

$$[1+\frac{1}{6}\delta^2-\frac{1}{2}(-c\,\Delta_0+d\,\delta^2)](U_j^{n+1}-U_j^n)=(-c\,\Delta_0+d\,\delta^2)U_j^n \tag{8}$$

where $c=a\Delta t/h$ is the Courant number and $d=\nu\Delta t/h^2$ the diffusion number. Here Δ_0 and δ^2 are the standard notations for the central difference operators:

$$\begin{aligned}\Delta_0 U_j &= \frac{1}{2}(U_{j+1}-U_{j-1})\\ \delta^2 U_j &= (U_{j+1}-2U_j+U_{j-1})\end{aligned} \tag{9}$$

To analyze the properties of the TG scheme (8), we substitute a Fourier mode e^{ikx} into it and, setting $\xi=kh$, find an amplification in one time step of

$$\begin{aligned}G_{TG}(\xi,c,d) &= 1+\frac{-ic\sin\xi-4d\sin^2\frac{1}{2}\xi}{1-(\frac{2}{3}-2d)\sin^2\frac{1}{2}\xi+\frac{1}{2}ic\sin\xi}\\ &= 1-ic\xi-(d+\frac{1}{2}c^2)\xi^2+ic(d+\frac{1}{4}c^2)\xi^3+\cdots \quad \text{as } \xi\to 0,\end{aligned} \tag{10}$$

where $\xi=kh$ is the dimensionless wave number, while k is the dimensional wave number of the Fourier mode e^{ikx}. G_{TG} is called the amplification factor of scheme (8) and it verifies $U_j^{n+1}/U_j^n=G_{TG}$.
The corresponding quantity for the differential equation is

$$G_{ex}=e^{-(\delta+i\,\omega)} \tag{11}$$

where $\delta=d\xi^2$ and $\omega=c\xi$ are the exact damping and frequency, respectively. From (10) it follows that this TG scheme is second-order accurate. To evaluate the accuracy of the scheme beyond the asymptotic limit, we introduce the damping δ_{num} and frequency ω_{num} of the fully discrete equations through the relation

$$G_{TG}=e^{-(\delta_{num}+i\,\omega_{num})} \tag{12}$$

which implies

$$\begin{aligned}\delta_{num} &= -\ln\mid G_{TG}\mid\\ \omega_{num} &= -\arg(G_{TG}).\end{aligned} \tag{13}$$

In Tables 1 and 2 the phase error $\Delta = \omega_{num}/\omega - 1$ and the damping ratio δ_{num}/δ for the TG scheme are compared with those of the Crank-Nicolson finite difference scheme (CN-FD) and the explicit Euler-Galerkin finite element scheme (EG-FE) which is only first order accurate.

From Table 1 one notes that the Taylor-Galerkin scheme shows a substantial improvement in phase speed with respect to the implicit finite difference scheme and the Euler finite element method. The values of the damping ratio in Table 2 indicate that the Taylor-Galerkin method reproduces very well the physical diffusion in the region of accurate spatial resolution ($0 \leq \xi \leq \frac{\pi}{4}$) and that it is overdiffusive in the high-frequency region where the phase-speed error is maximum. The Crank-Nicolson finite difference scheme is instead systematically underdiffusive, in particular for short wavelengths. Finally, the Euler finite element method has a rather limited stability interval and does not exhibit enough damping in the region of accuracy. Moreover, in the limit $\xi \to 0$ the damping ratio for Euler

c	d	ξ	$CN-FD$	$EG-FE$	$TG-FE$
		$\pi/4$	-0.1010	-0.0223	-0.0040
	0.05	$\pi/2$	-0.3639	-0.0800	-0.0497
		$3\pi/4$	-0.6982	-0.0562	-0.2829
		$\pi/4$	-0.1004	0.0571	-0.0032
0.2	0.1	$\pi/2$	-0.3592	0.2888	-0.0311
		$3\pi/4$	-0.6915	1.1360	-0.1888
		$\pi/4$	-0.0981	$--$	-0.0001
	0.2	$\pi/2$	-0.3395	$--$	0.0375
		$3\pi/4$	-0.6613	$--$	0.6122
		$\pi/4$	-0.1087	$--$	-0.0145
	0.05	$\pi/2$	-0.3748	$--$	-0.0822
		$3\pi/4$	-0.7009	$--$	-0.3187
		$\pi/4$	-0.1082	$--$	-0.0137
0.5	0.1	$\pi/2$	-0.3705	$--$	-0.0696
		$3\pi/4$	-0.6945	$--$	-0.2510
		$\pi/4$	-0.1060	$--$	-0.0108
	0.2	$\pi/2$	-0.3528	$--$	-0.0162
		$3\pi/4$	-0.6662	$--$	0.1263

Table 1: Phase errors Δ for fully discrete approximations to the advection-diffusion equation. Comparison between Taylor-Galerkin scheme with piecewise linear elements, Euler-Galerkin and Crank-Nicolson finite difference schemes.

c	d	ξ	$CN-FD$	$EG-FE$	$TG-FE$
		$\pi/4$	0.945	0.650	1.046
	0.05	$\pi/2$	0.803	0.841	1.191
		$3\pi/4$	0.613	1.351	1.406
		$\pi/4$	0.945	0.863	1.046
0.2	0.1	$\pi/2$	0.805	1.104	1.197
		$3\pi/4$	0.617	1.704	1.458
		$\pi/4$	0.946	—	1.047
	0.2	$\pi/2$	0.812	—	1.222
		$3\pi/4$	0.636	—	1.726
		$\pi/4$	0.920	—	1.014
	0.05	$\pi/2$	0.763	—	1.067
		$3\pi/4$	0.579	—	1.227
		$\pi/4$	0.921	—	1.014
0.5	0.1	$\pi/2$	0.765	—	1.069
		$3\pi/4$	0.601	—	1.242
		$\pi/4$	0.921	—	1.015
	0.2	$\pi/2$	0.770	—	1.080
		$3\pi/4$	0.617	—	1.248

Table 2: Damping ratios δ_{num}/δ for fully discrete approximations to the advection-diffusion equation. Comparison between Taylor-Galerkin scheme with piecewise linear elements, Euler-Galerkin and Crank-Nicolson finite difference schemes.

scheme is found to be $1 - c^2/2d$ instead of one. Therefore the diffusion of signals with long wavelengths is not correctly reproduced by this scheme unless $c^2/2d \to 0$, a condition which implies the use of exceedingly small time steps in advection-dominated problems.

3 New one-step TG schemes

In this section we introduce two new TG-schemes with good accuracy and stability properties for both convection and diffusion. These schemes can be seen as extensions of the second order explicit Taylor-Galerkin scheme TG corresponding to a Lax-Wendroff method (see [3]).

3.1 Time discretization

As in the previous section, we first consider the linear convection-diffusion equation for the scalar quantity u

$$u_t + \boldsymbol{a} \cdot \boldsymbol{\nabla} u = \nu \nabla^2 u \tag{14}$$

From (14) we have:

$$\begin{aligned} u_t^n &= -\boldsymbol{a} \cdot \boldsymbol{\nabla} u^n + \nu \nabla^2 u^n \\ u_{tt}^n &= (\boldsymbol{a} \cdot \boldsymbol{\nabla})^2 u^n + \nu \nabla^2 (u_t^n - \nu \nabla^2 u^n) + \nu \nabla^2 u_t^n \\ &= (\boldsymbol{a} \cdot \boldsymbol{\nabla})^2 u^n + 2\nu \nabla^2 \left(\frac{u^{n+1} - u^n}{\Delta t} \right) + O(\Delta t, \nu^2) \end{aligned} \tag{15}$$

Now, introducing (15) into the Taylor series expansion in time for u, we obtain the scheme

$$\left[1 - \Delta t \, \nu \nabla^2 \right] \frac{u^{n+1} - u^n}{\Delta t} = -\boldsymbol{a} \cdot \boldsymbol{\nabla} u^n + \nu \nabla^2 u^n + \frac{\Delta t}{2} (\boldsymbol{a} \cdot \boldsymbol{\nabla})^2 u^n \tag{16}$$

This is a new TG-algorithm (TG2C2D) for convection-diffusion problems. Its global accuracy is $O(\Delta t^2, \nu^2 \Delta t)$, but in general it has second order accuracy because usually $\nu^2 \leq \Delta t$. This method is identical to TG2 [3] for pure convection ($\nu = 0$). However, it represents a valuable extension of TG2 for convection-diffusion problems because, as will be seen in section 3.3, the new scheme retains the phase accuracy of TG2, but has a better stability when the diffusion dominates the transport process. The scheme (16) has the same drawbacks as TG2 for pure convection in that it has a strong stability restriction and exhibits some numerical dispersion. We can circunvent this problem by incorporating in the scheme a third order approximation of the convective term. This leads to a new improved scheme for convection-diffusion equations (TG3C2D) which reads:

$$\left[1 - \frac{\Delta t^2}{6} (\boldsymbol{a} \cdot \boldsymbol{\nabla})^2 - \Delta t \, \nu \nabla^2 \right] \frac{u^{n+1} - u^n}{\Delta t} = -\boldsymbol{a} \cdot \boldsymbol{\nabla} u^n + \nu \nabla^2 u^n + \frac{\Delta t}{2} (\boldsymbol{a} \cdot \boldsymbol{\nabla})^2 u^n \tag{17}$$

The global accuracy of scheme (17) is $O(\Delta t^3, \nu^2 \Delta t, \nu \Delta t^2)$. Usually $\nu^2 \leq \Delta t$, so the scheme is third order accurate as regards convection and second order accurate for diffusion. If $\nu \leq \Delta t$ the method is third order accurate. When $\nu = 0$, TG3C2D reduces to the classical TG3 scheme introduced in [3].

3.2 Spatial discretization

We apply the Galerkin formulation in space to obtain the fully discrete version of the previous schemes. We use the standard local interpolations in Eq.(6) with

linear or multilinear shape functions. Let Ω denote the domain of the problem, and $\Gamma = \partial\Omega$ its boundary.The scheme TG3C2D takes the form:

$$\begin{aligned}
&\textstyle\sum_j \Big[\langle N_j, N_i\rangle + \Delta t\,\nu\left(\langle \nabla N_j, \nabla N_i\rangle - \langle \boldsymbol{n}\cdot\nabla N_j, N_i\rangle_\Gamma\right)\\
&+ \tfrac{\Delta t^2}{6}\left(\langle \boldsymbol{a}\cdot\nabla N_j, \boldsymbol{a}\cdot\nabla N_i\rangle - \langle \boldsymbol{a}\cdot\nabla N_j, \boldsymbol{a}\cdot\boldsymbol{n}\, N_i\rangle_\Gamma\right)\Big]\,(U_j^{n+1} - U_j^n)/\Delta t =\\
&\textstyle\sum_j \Big[-\langle \boldsymbol{a}\cdot\nabla N_j, N_i\rangle\, U_j^n - \nu\,\langle \nabla N_j, \nabla N_i\rangle\, U_j^n\\
&+ \tfrac{\Delta t}{2}\left(-\langle \boldsymbol{a}\cdot\nabla N_j, \boldsymbol{a}\cdot\nabla N_i\rangle\, U_j^n + \langle \boldsymbol{a}\cdot\nabla N_j, \boldsymbol{a}\cdot\boldsymbol{n}\, N_i\rangle_\Gamma\, U_j^n\right)\\
&+ \nu\,\langle \boldsymbol{n}\cdot\nabla N_j, N_i\rangle_\Gamma\, U_j^n\Big]
\end{aligned}$$

A similar expression is obtained for TG2C2D.

3.3 Accuracy and stability analysis

If we use piecewise linear basis functions on a uniform mesh, the evolution of a Fourier component can be written in the form

$$U_{r,l}^{n+1} = G\,U_{r,l}^n$$

where $U_{r,l}^n = U(x_0 + rh,\, y_0 + lh,\, t_0 + n\Delta t)$ and G is the amplification factor (Δt and h are the time and spatial increments respectively). The numerical values of G are compared to the exact ones in Table 3, where
In 1D:

$$\begin{aligned}
c &= a\Delta t/h \quad \text{Courant number}\\
d &= \nu\Delta t/h^2 \quad \text{diffusion number}\\
\xi &= hk \quad \text{adimensional wave number}\\
M_0(\xi) &= 1 + \tfrac{1}{3}(\cos\xi - 1) \quad \text{consistent mass matrix}\\
A(\xi, c) &= ic\sin\xi \quad 1^{\text{st}} \text{ order convection term}\\
K(\xi, c) &= 2c^2(\cos\xi - 1) \quad 2^{\text{nd}} \text{ order convection term}\\
D(\xi, d) &= 2d(\cos\xi - 1) \quad 1^{\text{st}} \text{ order diffusion term}
\end{aligned}$$

	1D	2D
G_{ex}	$e^{-d\xi^2}e^{-ic\xi}$	$e^{-d\boldsymbol{\xi}\cdot\boldsymbol{\xi}}e^{-ic\cdot\boldsymbol{\xi}}$
G_{TG2C2D}	$1 + (D - A + K/2)/(M_0 - D)$	
G_{TG3C2D}	$1 + (D - A + K/2)/(M_0 - D - K/6)$	

Table 3: Structure of the amplification factors.

In 2D:

$$
\begin{aligned}
\boldsymbol{c} &= (c_1,\, c_2) = \boldsymbol{a}\Delta t/h \quad \text{Courant vector} \\
d &= \nu\Delta t/h^2 \quad \text{diffusion number} \\
\boldsymbol{\xi} &= (\xi,\, \eta) = h\boldsymbol{k} = h(k_1,\, k_2) \quad \text{adimensional wave vector} \\
M_0(\boldsymbol{\xi}) &= \tfrac{4}{9}\left(1+\tfrac{1}{2}\cos\xi\right)\left(1+\tfrac{1}{2}\cos\eta\right) \\
A(\boldsymbol{\xi},\boldsymbol{c}) &= i\tfrac{2}{3}\left[c_1\sin\xi\left(1+\tfrac{1}{2}\cos\eta\right)+c_2\sin\eta\left(1+\tfrac{1}{2}\cos\xi\right)\right] \\
K(\boldsymbol{\xi},\boldsymbol{c}) &= \tfrac{4}{3}\left[c_1^2\left(1+\tfrac{1}{2}\cos\eta\right)(\cos\xi-1)+c_2^2\left(1+\tfrac{1}{2}\cos\xi\right)(\cos\eta-1)\right] \\
&\quad -2c_1c_2\sin\xi\sin\eta \\
D(\boldsymbol{\xi},d) &= \tfrac{4}{3}d\left[\left(1+\tfrac{1}{2}\cos\eta\right)(\cos\xi-1)+\left(1+\tfrac{1}{2}\cos\xi\right)(\cos\eta-1)\right] \\
&\quad -2d\sin\xi\sin\eta
\end{aligned}
$$

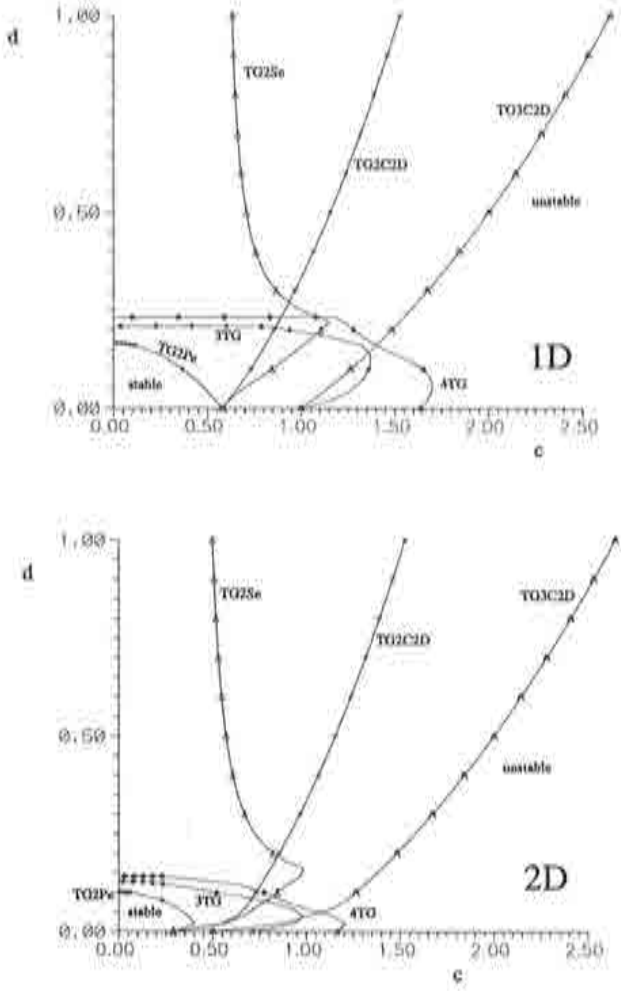

Figure 1: Stability limits in 1D and 2D. ($Pe = c/d$ is the Péclet number).

dim.	method	G/G_{ex}
1D	TG2C2D	$1 - \frac{i}{6} c^3 \xi^3 + O(\xi^4)$
1D	TG3C2D	$1 + O(\xi^4)$
2D	TG2C2D	$1 - 2d\xi\eta - \frac{i}{6} c_1^3 \xi^3 - \frac{i}{6} c_2^3 \eta^3 - \frac{i}{2} c_1^2 c_2 \xi^2 \eta - \frac{i}{2} c_1 c_2^2 \xi \eta^2 + O(\xi^4)$
2D	TG3C2D	$1 - 2d\xi\eta + O(\xi^4)$

Table 4: Spatial order of accuracy.

dimension	method	convection
1D	TG2C2D	$1/\sqrt{3}$
1D	TG3C2D	1
2D	TG2C2D	0.28884
2D	TG3C2D	0.50029

Table 5: Stability limits in pure convection.

The stability limits of schemes TG2C2D and TG3C2D in 1D and 2D are shown in Fig. 1 and Table 5.
One notes that TG2C2D and TG3C2D improve the stability limit of the usual second-order TG methods and maintain a good phase accuracy when diffusion increases (see Figs. 1-3 and Tables 6 and 7). Only the damping ratio becomes sligthly less accurate with increasing diffusion for high frequencies. For a more complete comparison we also show in Fig. 1 the stability limits of three other explicit methods. The first is a three-stage third-order TG scheme (3TG) [15, 16]. The second is a one-step second-order (for convection) TG scheme (TG2Pe) [19, 20], while the third method is a two-step scheme with operator splitting (TG2Se) [25]. Also, these three methods suffer from a reduced accuracy when diffusion is important. As an illustration, we have reported in Fig. 3 the response of 3TG and TG2Pe.
The spatial accuracy of the new methods can be appraised from Table 4. TG2C2D and TG3C2D are third and fourth order accurate, respectively, in 1D. In 2D a diffusive term $(-2d\xi\eta)$ appears which degrades the damping response, but not the phase since the additional term is real. This term comes from the use of a consistent mass matrix.

c	d	ξ	$TG2C2D$	$TG3C2D$	$TG-FE$	$3TG$
		$\pi/8$	$+0.0009$	-0.0001	-0.0006	-0.0001
		$\pi/4$	$+0.0025$	-0.0018	-0.0043	-0.0023
0.2	0	$\pi/2$	-0.0166	-0.0359	-0.0521	-0.0448
		$3\pi/4$	-0.2110	-0.2538	-0.3098	-0.3034
		$\pi/8$	$+0.0009$	-0.0001	-0.0006	-0.0001
		$\pi/4$	$+0.0025$	-0.0018	-0.0040	-0.0024
0.2	0.05	$\pi/2$	-0.0166	-0.0359	-0.0497	-0.0470
		$3\pi/4$	-0.2110	-0.2538	-0.2829	-0.3027
		$\pi/8$	$+0.0009$	-0.0001	-0.0006	-0.0001
		$\pi/4$	$+0.0025$	-0.0018	-0.0033	-0.0025
0.2	0.1	$\pi/2$	-0.0166	-0.0359	-0.0311	-0.0464
		$3\pi/4$	-0.2110	-0.2538	-0.1888	-0.2172
		$\pi/8$	$+0.0009$	-0.0001	-0.0004	-0.0002
		$\pi/4$	$+0.0025$	-0.0018	-0.0001	-0.0025
0.2	0.2	$\pi/2$	-0.0166	-0.0359	$+0.0375$	-0.0077
		$3\pi/4$	-0.2110	-0.2538	$+0.6122$	1.3727
		$\pi/8$	$+0.0065$	0.0000	-0.0033	-0.0001
		$\pi/4$	$+0.0264$	0.0000	-0.0148	-0.0015
0.5	0	$\pi/2$	$+0.1154$	0.0000	-0.0864	-0.0356
		$3\pi/4$	$+0.3233$	0.0000	-0.3392	-0.2938
		$\pi/8$	$+0.0065$	0.0000	-0.0033	-0.0001
		$\pi/4$	$+0.0264$	0.0000	-0.0145	-0.0023
0.5	0.05	$\pi/2$	$+0.1154$	0.0000	-0.0822	-0.0489
		$3\pi/4$	$+0.3233$	0.0000	-0.3187	-0.3343
		$\pi/8$	$+0.0065$	0.0000	-0.0033	-0.0002
		$\pi/4$	$+0.0264$	0.0000	-0.0138	-0.0032
0.5	0.1	$\pi/2$	$+0.1154$	0.0000	-0.0696	-0.0680
		$3\pi/4$	$+0.3233$	0.0000	-0.2510	-0.3730
		$\pi/8$	$+0.0065$	0.0000	-0.0031	-0.0003
		$\pi/4$	$+0.0264$	0.0000	-0.0108	-0.0051
0.5	0.2	$\pi/2$	$+0.1154$	0.0000	-0.0162	-0.1066
		$3\pi/4$	$+0.3233$	0.0000	$+0.1263$	-0.0229

Table 6: Phase errors Δ for fully discrete approximations to the advection-diffusion equation. Comparison between Taylor-Galerkin scheme with piecewise linear elements TG-FE, 3TG, and the new schemes TG2C2D and TG3C2D.

c	d	ξ	$TG2C2D$	$TG3C2D$	$TG-FE$	$3TG$
		$\pi/8$	1.000	1.000	1.000	1.000
		$\pi/4$	0.999	0.999	1.000	1.000
0.2	0	$\pi/2$	0.987	0.986	1.000	1.000
		$3\pi/4$	0.903	0.905	1.000	0.999
		$\pi/8$	1.013	1.013	1.011	1.013
		$\pi/4$	1.056	1.053	1.046	1.053
0.2	0.05	$\pi/2$	1.241	1.226	1.191	1.216
		$3\pi/4$	1.569	1.511	1.406	1.413
		$\pi/8$	1.007	1.006	1.011	1.013
		$\pi/4$	1.030	1.026	1.046	1.053
0.2	0.1	$\pi/2$	1.118	1.102	1.197	1.210
		$3\pi/4$	1.234	1.191	1.458	1.405
		$\pi/8$	0.998	0.998	1.011	1.013
		$\pi/4$	0.994	0.991	1.047	1.052
0.2	0.2	$\pi/2$	0.980	0.966	1.222	1.202
		$3\pi/4$	0.947	0.917	1.726	1.373
		$\pi/8$	1.000	1.000	1.000	1.000
		$\pi/4$	0.998	0.997	1.000	0.999
0.5	0	$\pi/2$	0.976	0.943	1.000	0.989
		$3\pi/4$	0.820	0.668	1.000	0.985
		$\pi/8$	1.017	1.027	1.003	1.021
		$\pi/4$	1.071	1.110	1.014	1.086
0.5	0.05	$\pi/2$	1.327	1.492	1.067	1.344
		$3\pi/4$	1.915	2.395	1.227	1.485
		$\pi/8$	1.009	1.011	1.003	1.017
		$\pi/4$	1.037	1.044	1.014	1.069
0.5	0.1	$\pi/2$	1.160	1.197	1.069	1.271
		$3\pi/4$	1.407	1.569	1.242	1.253
		$\pi/8$	0.999	0.997	1.003	1.015
		$\pi/4$	0.998	0.990	1.015	1.059
0.5	0.2	$\pi/2$	1.001	0.986	1.080	1.157
		$3\pi/4$	1.033	1.070	1.248	0.621

Table 7: Damping ratios δ_{num}/δ for fully discrete approximations to the advection-diffusion equation. Comparison between Taylor-Galerkin scheme with piecewise linear elements TG-FE, 3TG, and the new schemes TG2C2D and TG3C2D.

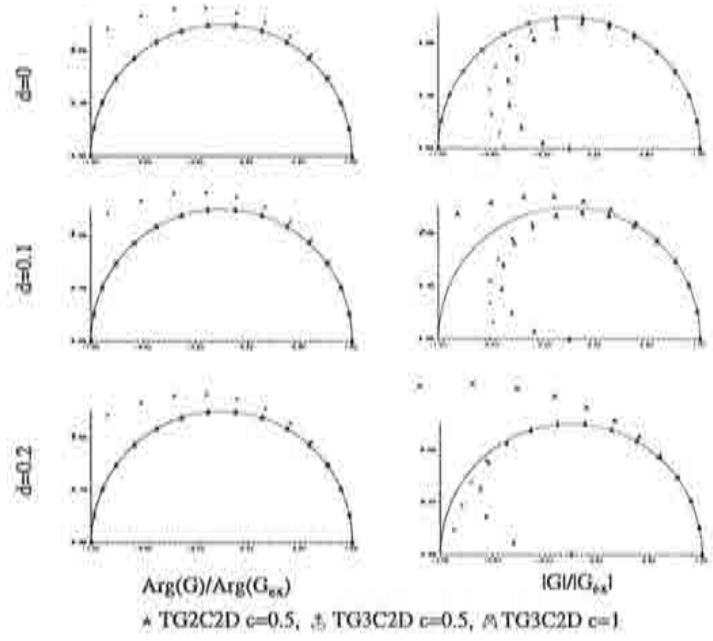

Figure 2: Relative errors of TG2C2D and TG3C2D in 1D.

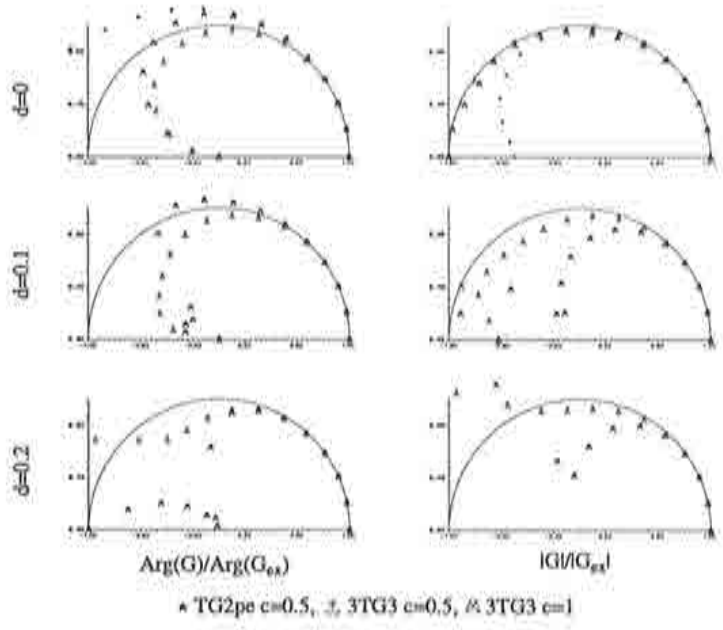

Figure 3: Relative errors of TG2Pe and 3TG in 1D.

4 Multi-stage approach to Padé approximations

4.1 Introduction

From the forward Taylor series developement

$$\begin{aligned} u^{n+1} &= \left(1 + \Delta t\frac{\partial}{\partial t} + \frac{1}{2!}\Delta t^2\frac{\partial^2}{\partial t^2} + \frac{1}{3!}\Delta t^3\frac{\partial^3}{\partial t^3} + \ldots\right) u^n \\ &= \exp\left(\Delta t\frac{\partial}{\partial t}\right) u^n, \end{aligned} \tag{18}$$

it is apparent that time-stepping schemes of various orders of accuracy can be devised in the form of Padé approximations [9, 21] for the exponential function. A Padé approximation to the exponential function e^x, where in the present context $x = \Delta t\frac{\partial}{\partial t}$, is the quotient of two polynomials $P_n(x)$ and $Q_m(x)$ of degrees n and m, respectively. We use the notation $R_{n,m}$ to denote this quotient. Padé approximations to e^x up to order $n + m = 6$ are shown in Table 8 in which classical explicit and implicit time integration methods are easily recognized.
As already mentioned in the Introduction, higher-order time integration methods for the convection–diffusion equation should only involve the first time derivative of the unknown if they are to be easily implemented in standard finite element codes using elements with C^0 continuity for linear and non linear problems.
With the view of integrating advection-diffusion equations forward in time using first time derivatives only, we shall now look at ways of reproducing higher-order Padé approximantions through a multi-stage process. Explicit methods of order two, three, and four corresponding to approximantions $R_{2,0}$, $R_{3,0}$ and $R_{4,0}$ will be considered first. Then, multi-stage schemes corresponding to implicit Padé approximations of order two to six will be examined. Finally the Padé schemes are specialized to deal with pure advection problems.

4.2 Explicit multi-stage methods

4.2.1 Second order scheme

Let us consider first the second-order time integration scheme corresponding to the explicit Padé approximation $R_{2,0}$ in Table 8. The scheme reads

$$u^{n+1} = u^n + \Delta t\, u_t^n + \tfrac{1}{2}\Delta t^2\, u_{tt}^n \tag{19}$$

and corresponds to the well-known Lax-Wendroff method.
To avoid second time derivatives which are difficult to express in terms of the spatial derivatives in the advection-diffusion equation, a two-step approach to this second order explicit scheme has been proposed by Richtmyer (see [22]) in the form

$$u^{n+\frac{1}{2}} = u^n + \tfrac{1}{2}\Delta t\, u_t^n$$

$$u^{n+1} = u^n + \Delta t\, u_t^{n+\frac{1}{2}} \tag{20}$$

which emanates from the factorization of Padé approximation $R_{2,0}$ in the form

$$1 + x + \tfrac{1}{2}x^2 = 1 + x\left(1 + \tfrac{1}{2}x\right) \tag{21}$$

The two-step Lax-Wendroff method is only conditionally stable.

4.2.2 Third-order scheme

Considering now Padé approximation $R_{3,0}$ in Table 8, three stages are needed to reproduce it using first time derivatives only. The three-stage explicit method corresponds to the nested factorization of $R_{3,0}$:

$$\begin{aligned} 1 + x + \tfrac{1}{2}x^2 + \tfrac{1}{6}x^3 &= 1 + x\left(1 + \tfrac{1}{2}x + \tfrac{1}{6}x^2\right) \\ &= 1 + x\left(1 + \tfrac{1}{2}x(1 + \tfrac{1}{3}x)\right) \end{aligned} \tag{22}$$

which produces the three-stage scheme

$$\begin{aligned} u^{n+\frac{1}{3}} &= u^n + \tfrac{1}{3}\Delta t\, u_t^n \\ u^{n+\frac{1}{2}} &= u^n + \tfrac{1}{2}\Delta t\, u_t^{n+\frac{1}{3}} \\ u^{n+1} &= u^n + \Delta t\, u_t^{n+\frac{1}{2}} \end{aligned} \tag{23}$$

This third-order explicit scheme has been employed in references [15] and [16] in the finite element solution of incompressible flow problems. Like all methods above the diagonal in Table 8, the third-order scheme corresponding to $R_{3,0}$ is only conditionally stable.

4.2.3 Fourth-order scheme

Looking now at the explicit Padé approximation $R_{4,0}$, four stages are needed to reproduce it using first time derivatives only. The four-stage explicit method corresponds to the nested factorization of $R_{4,0}$:

$$\begin{aligned} 1 + x + \tfrac{1}{2}x^2 + \tfrac{1}{6}x^3 + \tfrac{1}{24}x^4 &= 1 + x\left(1 + \tfrac{1}{2}x + \tfrac{1}{6}x^2 + \tfrac{1}{24}x^3\right) \\ &= 1 + x\left(1 + \tfrac{1}{2}x(1 + \tfrac{1}{3}x + \tfrac{1}{12}x^2)\right) \\ &= 1 + x\left(1 + \tfrac{1}{2}x\left(1 + \tfrac{1}{3}(1 + \tfrac{1}{4}x)\right)\right) \end{aligned} \tag{24}$$

which produces the four-stage explicit method

$$\begin{aligned} u^{n+\frac{1}{4}} &= u^n + \tfrac{1}{4}\Delta t\, u_t^n \\ u^{n+\frac{1}{3}} &= u^n + \tfrac{1}{3}\Delta t\, u_t^{n+\frac{1}{4}} \\ u^{n+\frac{1}{2}} &= u^n + \tfrac{1}{2}\Delta t\, u_t^{n+\frac{1}{3}} \\ u^{n+1} &= u^n + \Delta t\, u_t^{n+\frac{1}{2}} \end{aligned} \tag{25}$$

$R_{n,m}(x)$	$n=0$	$n=1$	$n=2$	$n=3$
$m=0$	1	$1+x$	$1+x+\frac{1}{2}x^2$	$1+x+\frac{1}{2}x^2+\frac{1}{6}x^3$
$m=1$	$\frac{1}{1-x}$	$\frac{1+\frac{1}{2}x}{1-\frac{1}{2}x}$	$\frac{1+\frac{2}{3}x+\frac{1}{6}x^2}{1-\frac{1}{3}x}$	$\frac{1+\frac{3}{4}x+\frac{1}{4}x^2+\frac{1}{24}x^3}{1-\frac{1}{4}x}$
$m=2$	$\frac{1}{1-x+\frac{1}{2}x^2}$	$\frac{1+\frac{1}{3}x}{1-\frac{2}{3}x+\frac{1}{6}x^2}$	$\frac{1+\frac{1}{2}x+\frac{1}{12}x^2}{1-\frac{1}{2}x+\frac{1}{12}x^2}$	$\frac{1+\frac{3}{5}x+\frac{3}{20}x^2+\frac{1}{60}x^3}{1-\frac{2}{5}x+\frac{1}{20}x^2}$
$m=3$	$\frac{1}{1-x+\frac{1}{2}x^2-\frac{1}{6}x^3}$	$\frac{1+\frac{1}{4}x}{1-\frac{3}{4}x+\frac{1}{4}x^2-\frac{1}{24}x^3}$	$\frac{1+\frac{2}{5}x+\frac{1}{20}x^2}{1-\frac{3}{5}x+\frac{3}{20}x^2-\frac{1}{60}x^3}$	$\frac{1+\frac{1}{2}x+\frac{1}{10}x^2+\frac{1}{120}x^3}{1-\frac{1}{2}x+\frac{1}{10}x^2-\frac{1}{120}x^3}$

Table 8: Padé approximations of the exponential function e^x.

The method is again conditionally stable and presents, as we shall see similarities with the fourth-order explicit Runge-Kutta method discussed in Section 6.

4.3 Implicit multi-stage methods

We shall now consider implicit multi-stage methods for the advection-diffusion equation emanating from Padé approximations in Table 8 corresponding to $m \neq 0$. We shall see that not all implicit methods deriving from Padé approximations with $m \neq 0$ are unconditionally stable in application to the linear advection-diffusion equation. Actually, it appears (as could be expected) that only those implicit Padé approximations which are on or below the diagonal in Table 8, i.e., the $R_{n,m}$ with $m \geq n$, do possess interesting stability properties.

4.3.1 Second-order implicit methods

Approximation $R_{1,1}$

Approximation $R_{1,1}$ in Table 8 reads

$$\left(1 - \frac{x}{2}\right) u^{n+1} = \left(1 + \frac{x}{2}\right) u^n \tag{26}$$

and corresponds to the second-order accurate Crank-Nicolson method

$$u^{n+1} = u^n + \tfrac{1}{2}\Delta t \left(u_t^n + u_t^{n+1}\right) \tag{27}$$

A two-step version of this implicit scheme is obtained in the form

$$\begin{array}{lll} u^{n+\frac{1}{2}} & = \left(1 + \frac{x}{2}\right) u^n & = u^n + \frac{\Delta t}{2} u_t^n \\ u^{n+1} & = u^{n+\frac{1}{2}} + \frac{x}{2} u^{n+1} & = u^{n+\frac{1}{2}} + \frac{\Delta t}{2} u_t^{n+1} \end{array}$$

This two-step version of the Crank-Nicolson scheme clearly presents no interest with respect to the one-step scheme. It simply shows in an elementary way how multi-stage schemes consisting of an explicit predictor followed by an implicit corrector can be constructed from implicit Padé approximations $R_{n,m}$.

Approximation $R_{0,2}$

Let us now consider the second-order implicit approximation $R_{0,2}$ which corresponds to the scheme:

$$\left(1 - x(1 - \tfrac{x}{2})\right) u^{n+1} = u^n \tag{28}$$

A two-stage version of this scheme is obtained by defining the intermediate value

$$u^{n+\frac{1}{2}} = (1 - \tfrac{x}{2})\, u^{n+1} \tag{29}$$

which allows to write the $R_{0,2}$ method in the form

$$\begin{aligned} u^{n+\frac{1}{2}} &= \left(1 - \frac{x}{2}\right) u^{n+1} \\ u^{n+1} &= u^n + x\, u^{n+\frac{1}{2}} \end{aligned} \tag{30}$$

of two coupled equations governing the unknowns $u^{n+\frac{1}{2}}$ and u^{n+1} and involving first time derivatives only.

4.3.2 Third-order implicit methods

Considering now implicit methods of third order, we note from Table 8 that they correspond to approximations $R_{2,1}$, $R_{1,2}$ and $R_{0,3}$.

Approximation $R_{2,1}$
Considering first approximation $R_{2,1}$, we see that it generates the time integration scheme

$$\begin{aligned} \left(1 - \frac{x}{3}\right) u^{n+1} &= \left(1 + \frac{2}{3}x + \frac{x^2}{6}\right) u^n \\ &= \left(1 + \frac{2}{3}x\left(1 + \frac{x}{4}\right)\right) u^n \end{aligned} \tag{31}$$

which can be decomposed into the following two-stage third-order method consisting of an explicit predictor followed by an implicit corrector:

$$\begin{aligned} u^{n+\frac{1}{4}} &= u^n + \frac{\Delta t}{4} u_t^n \\ u^{n+1} &= u^n + \frac{\Delta t}{3}\left(2\, u_t^{n+\frac{1}{4}} + u_t^{n+1}\right) \end{aligned} \tag{32}$$

Approximation $R_{1,2}$
Looking now at approximation $R_{1,2}$, we see that it produces the implicit time integration method

$$\left(1 - \frac{2}{3}x(1 - \frac{x}{4})\right) u^{n+1} = \left(1 + \frac{x}{3}\right) u^n \tag{33}$$

which, defining the intermediate value

$$\tilde{u} = \left(1 - \frac{x}{4}\right) u^{n+1} \tag{34}$$

yields the following pair of implicit equations

$$\begin{aligned} u^{n+1} - \tilde{u} &= \frac{\Delta t}{4} u_t^{n+1} \\ u^{n+1} - u^n &= \frac{\Delta t}{3}\left(u_t^n + 2\,\tilde{u}_t\right) \end{aligned} \tag{35}$$

Approximation $R_{0,3}$
Another third-order method is provided by approximation $R_{0,3}$ in Table 8 which generates the fully implicit scheme

$$\left(1 - x + \frac{x^2}{2} - \frac{x^3}{6}\right) u^{n+1} = u^n. \tag{36}$$

which we rewrite in the form

$$\left(1 - x\left(1 - \frac{x}{2}(1 - \frac{x}{3})\right)\right) u^{n+1} = u^n. \tag{37}$$

Defining the intermediate quantities

$$\begin{aligned} \tilde{u} &= u^{n+1} - \frac{\Delta t}{3} u_t^{n+1} \\ \hat{u} &= u^{n+1} - \frac{\Delta t}{2} \tilde{u}_t \end{aligned} \tag{38}$$

the above scheme leads to the following system of coupled equations

$$\begin{aligned} \tilde{u} &= u^{n+1} - \frac{\Delta t}{3} u_t^{n+1} \\ \hat{u} &= u^{n+1} - \frac{\Delta t}{2} \tilde{u}_t \\ u^{n+1} &= u^n + \hat{u}_t \end{aligned} \tag{39}$$

4.3.3 Fourth-order implicit methods

These methods correspond to Padé approximations $R_{2,2}$, $R_{3,1}$ and $R_{1,3}$.

Approximation $R_{2,2}$
The implicit method corresponding to $R_{2,2}$ reads

$$\left(1 - \frac{x}{2}(1 - \frac{x}{6})\right) u^{n+1} = \left(1 + \frac{x}{2}(1 + \frac{x}{6})\right) u^n \tag{40}$$

From this expression we deduce the following 4-stage method incorporating two explicit predictors and two implicit correctors:

$$\begin{aligned} u^{n+\frac{1}{6}} &= u^n + \frac{\Delta t}{6} u_t^n \\ u^{n+\frac{1}{2}} &= u^n + \frac{\Delta t}{2} u_t^{n+\frac{1}{6}} \\ \tilde{u} &= u^{n+1} - \frac{\Delta t}{6} u_t^{n+1} \\ u^{n+1} &= u^{n+\frac{1}{2}} + \frac{\Delta t}{2} \tilde{u}_t \end{aligned} \tag{41}$$

Approximation $R_{3,1}$

Looking now at Padé approximation $R_{3,1}$ in Table 8, we see that it generates the time integration scheme

$$\left(1-\frac{x}{4}\right)u^{n+1} = \left(1+\frac{3}{4}x\left(1+\frac{x}{3}(1+\frac{x}{6})\right)\right)u^n \tag{42}$$

Therefore, the fourth-order method arising from $R_{3,1}$ can be implemented in the form of three explicit stages

$$\begin{aligned} u^{n+\frac{1}{6}} &= u^n + \frac{\Delta t}{6}u_t^n \\ u^{n+\frac{1}{3}} &= u^n + \frac{\Delta t}{3}u_t^{n+\frac{1}{6}} \\ u^{n+\frac{3}{4}} &= u^n + \frac{3}{4}\Delta t\, u_t^{n+\frac{1}{3}} \end{aligned} \tag{43}$$

followed by the implicit stage

$$u^{n+1} = u^{n+\frac{3}{4}} + \frac{\Delta t}{4}u_t^{n+1} \tag{44}$$

Approximation $R_{1,3}$

Similarly, from the Padé approximation $R_{1,3}$ we obtain the following fourth-order implicit scheme

$$\left(1-\frac{3}{4}x\left(1-\frac{x}{3}(1-\frac{x}{6})\right)\right)u^{n+1} = \left(1+\frac{x}{4}\right)u^n \tag{45}$$

which can be implemented in the form of one explicit stage followed by three implicit stages as follows

$$\begin{aligned} u^{n+\frac{1}{4}} &= u^n + \frac{\Delta t}{4}u^n \\ u^{n+1} - \frac{\Delta t}{6}u_t^{n+1} &= \hat{u} \\ u^{n+1} - \frac{\Delta t}{3}\hat{u}_t &= \hat{u} \\ u^{n+1} - \frac{3}{4}\Delta t\,\hat{u}_t &= u^{n+\frac{1}{4}} \end{aligned} \tag{46}$$

4.3.4 Fifth-order implicit methods

Approximation $R_{3,2}$

Let us now consider the fifth-order implicit approximation $R_{3,2}$ which corresponds to the scheme:

$$\left(1-\frac{2}{5}x(1-\frac{1}{8}x)\right)u^{n+1} = \left(1+\frac{3}{5}x\left(1+\frac{1}{4}x(1+\frac{1}{9}x)\right)\right)u^n \tag{47}$$

Therefore, it can be implemented in the form of three explicit stages

$$\begin{aligned} u^{n+\frac{1}{9}} &= u^n + \frac{\Delta t}{9} u_t^n \\ u^{n+\frac{1}{4}} &= u^n + \frac{\Delta t}{4} u_t^{n+\frac{1}{9}} \\ u^{n+\frac{3}{5}} &= u^n + \frac{3}{5}\Delta t\, u_t^{n+\frac{1}{4}} \end{aligned} \tag{48}$$

followed by two implicit ones

$$\begin{aligned} u^{n+1} - \frac{\Delta t}{8} u_t^{n+1} &= \tilde{u} \\ u^{n+1} &= u^{n+\frac{3}{5}} + \frac{2\Delta t}{5}\tilde{u}_t \end{aligned} \tag{49}$$

Approximation $R_{2,3}$

Approximation $R_{2,3}$ in Table 8 generates the folowing time integration scheme

$$\left(1 - \frac{3}{5}x\left(1 - \frac{1}{4}x(1 - \frac{1}{9}x)\right)\right) u^{n+1} = \left(1 + \frac{2}{5}x(1 + \frac{1}{8}x)\right) u^n. \tag{50}$$

From this expression we deduce the following 5-stage method incorporating two explicit predictors and three implicit correctors:

$$\begin{aligned} u^{n+\frac{1}{8}} &= u^n + \frac{\Delta t}{8} u_t^n \\ u^{n+\frac{2}{5}} &= u^n + \frac{2\Delta t}{5} u_t^{n+\frac{1}{8}} \end{aligned} \tag{51}$$

$$\begin{aligned} u^{n+1} - \frac{\Delta t}{9} u_t^{n+1} &= \hat{u} \\ u^{n+1} - \frac{\Delta t}{4}\hat{u}_t &= \hat{u} \\ u^{n+1} - \frac{3\Delta t}{5}\hat{u}_t &= u^{n+\frac{2}{5}} \end{aligned} \tag{52}$$

4.3.5 A sixth-order implicit scheme

Approximation $R_{3,3}$ in Table 8 produces the time scheme

$$\frac{u^{n+1} - u^n}{\Delta t} = \frac{1}{2}\left(u_t^n + u_t^{n+1}\right) + \frac{\Delta t}{10}\left(u_{tt}^n - u_{tt}^{n+1}\right) + \frac{\Delta t^2}{120}\left(u_{ttt}^n + u_{ttt}^{n+1}\right), \tag{53}$$

which is sixth-order accurate in the time step Δt. To implement such a scheme a multi-stage approach is needed which is based upon the nested factorization of $R_{3,3}$

$$\left(1 - \frac{x}{2}\left(1 - \frac{x}{5}(1 - \frac{x}{12})\right)\right) u^{n+1} = \left(1 + \frac{x}{2}\left(1 + \frac{x}{5}(1 + \frac{x}{12})\right)\right) u^n \tag{54}$$

This leads to three explicit stages

$$\begin{aligned} u^{n+\frac{1}{12}} &= u^n + \frac{\Delta t}{12} u_t^n \\ u^{n+\frac{1}{5}} &= u^n + \frac{\Delta t}{5} u_t^{n+\frac{1}{12}} \\ u^{n+\frac{1}{2}} &= u^n + \frac{\Delta t}{2} u_t^{n+\frac{1}{5}} \end{aligned} \tag{55}$$

followed by three implicit stages

$$\begin{aligned} u^{n+1} - \frac{\Delta t}{12} u_t^{n+1} &= \tilde{u} \\ u^{n+1} - \frac{\Delta t}{5} \tilde{u}_t &= \hat{u} \\ u^{n+1} - \frac{\Delta t}{2} \hat{u}_t &= u^{n+\frac{1}{2}} \end{aligned} \tag{56}$$

4.4 Multi-stage schemes for pure convection

When dealing with pure convection problems it is generally possible to express the second time derivative of the unknown in terms of spatial derivatives. It follows that multi-stage schemes incorporating both first and second time derivatives might prove useful for solving problems describing purely convective transport.

4.4.1 Third-order methods

Approximation $R_{3,0}$
Considering first the explicit approximation $R_{3,0}$, the factorization

$$\begin{aligned} u^{n+1} &= \left(1 + x + \frac{x^2}{2} + \frac{x^3}{6}\right) u^n \\ &= \left(1 + x + \frac{x^2}{2}(1 + \frac{x}{3})\right) u^n \end{aligned} \tag{57}$$

leads to the following two-stage explicit method

$$\begin{aligned} u^{n+\frac{1}{3}} &= u^n + \frac{\Delta t}{3} u_t^n \\ u^{n+1} &= u^n + \Delta t\, u_t^n + \frac{1}{2} \Delta t^2 u_u^{n+\frac{1}{3}} \end{aligned} \tag{58}$$

One can also decompose $R_{3,0}$ in the form

$$u^{n+1} = \left(1 + x(1 + \frac{x}{2} + \frac{x^2}{6})\right) u^n \tag{59}$$

which leads to the alternative third-order explicit scheme:

$$\begin{aligned} u^{n+\frac{1}{2}} &= u^n + \frac{\Delta t}{2} u_t^n + \frac{\Delta t^2}{6} u_{tt}^n \\ u^{n+1} &= u^n + \Delta t\, u_t^{n+\frac{1}{2}} \end{aligned} \tag{60}$$

Approximation $R_{2,1}$ and $R_{1,2}$

In the case of approximant $R_{2,1}$, the following one-stage implicit method is obtained

$$u^{n+1} = u^n + \frac{\Delta t}{3}\left(u_t^{n+1} + 2u_t^n\right) + \frac{\Delta t^2}{6} u_{tt}^n \tag{61}$$

Similarly, the third-order implicit method corresponding to $R_{1,2}$ reads

$$u^{n+1} = u^n + \frac{\Delta t}{3}\left(u_t^n + 2u_t^{n+1}\right) - \frac{\Delta t^2}{6} u_{tt}^{n+1} \tag{62}$$

Approximation $R_{0,3}$

Finally, in the case of the fully implicit approximant $R_{0,3}$, the following factorizations can be used

$$\begin{aligned} \left(1 - x + \frac{x^2}{2}(1 - \frac{x}{3})\right) u^{n+1} &= u^n \\ \left(1 - x(1 - \frac{x}{2} + \frac{x^2}{6})\right) u^{n+1} &= u^n, \end{aligned} \tag{63}$$

The first leads to the two-stage scheme

$$\begin{aligned} \tilde{u} &= u^{n+1} - \frac{\Delta t}{3} u_t^{n+1} \\ u^{n+1} - \Delta t\, u_t^{n+1} + \frac{\Delta t^2}{2} \tilde{u}_{tt} &= u^n, \end{aligned} \tag{64}$$

while the second gives

$$\begin{aligned} \tilde{u} &= (1 - \frac{x}{2} + \frac{x^2}{6})\, u^{n+1} \\ u^{n+1} - \Delta t\, \tilde{u}_t &= u^n, \end{aligned} \tag{65}$$

4.4.2 Fourth-order methods

Approximation $R_{2,2}$
Approximation $R_{2,2}$, which represents the fourth-order implicit scheme of Harten and Tal-Ezer [11] can be used directly in pure advection problems. The resulting time integration method reads

$$u^{n+1} = u^n + \frac{\Delta t}{2}\left(u_t^n + u_t^{n+1}\right) + \frac{\Delta t^2}{12}\left(u_{tt}^n - u_{tt}^{n+1}\right) \quad . \tag{66}$$

and its application in combination with linear elements for spatial discretization has been discussed in [3].
Two additional fourth-order schemes are provided by Padé approximations $R_{3,1}$ and $R_{1,3}$.

Approximation $R_{3,1}$
In the case of $R_{3,1}$ the following method is obtained which consists of two explicit stages followed by an implicit one:

$$\begin{aligned} u^{n+\frac{1}{3}} &= u^n + \frac{\Delta t}{3}u_t^n + \frac{\Delta t^2}{18}u_{tt}^n \\ u^{n+\frac{3}{4}} &= u^n + \frac{3}{4}\Delta t\, u_t^{n+\frac{1}{3}} \\ u^{n+1} &= u^{n+\frac{3}{4}} + \frac{\Delta t}{4}u_t^{n+1} \end{aligned} \tag{67}$$

Approximation $R_{1,3}$
Considering now approximation $R_{1,3}$, we see from Table 8 that it can be implemented for pure convection in the form of one explicit stage followed by two implicit ones as follows:

$$\begin{aligned} u^{n+\frac{1}{4}} &= u^n + \frac{\Delta t}{4}u_t^n \\ \tilde{u} &= u^{n+1} - \frac{\Delta t}{3}u_t^{n+1} + \frac{\Delta t^2}{18}u_{tt}^{n+1} \\ u^{n+1} &= u^{n+\frac{1}{4}} + \frac{3}{4}\Delta t\, \tilde{u}_t \end{aligned} \tag{68}$$

4.4.3 Fifth-order methods

Approximation $R_{3,2}$
Approximation $R_{3,2}$ generates the time integration scheme

$$\left(1 - \frac{2}{5}x + \frac{1}{20}x^2\right)u^{n+1} = \left(1 + \frac{3}{5}x(1 + \frac{1}{4}x + \frac{1}{36}x^2)\right)u^n \tag{69}$$

which can be decomposed into the form of two explicit stages

$$\begin{aligned} u^{n+\frac{1}{4}} &= u^n + \frac{\Delta t}{4} u_t^n + \frac{\Delta t^2}{36} u_{tt}^n \\ u^{n+\frac{3}{5}} &= u^n + \frac{3}{5}\Delta t\, u_t^{n+\frac{1}{4}} \end{aligned} \tag{70}$$

followed by one implicit stage

$$u^{n+1} - \frac{2\Delta t}{5} u_t^{n+1} + \frac{\Delta t^2}{20} u_{tt}^{n+1} = u^{n+\frac{3}{5}} \tag{71}$$

Approximation $R_{2,3}$

Approximation $R_{2,3}$ in Table 8 represents a fifth-order accurate implicit method. It can be factorized in the form

$$\left(1 - \frac{3}{5}x(1 - \frac{1}{4}x + \frac{1}{36}x^2)\right) u^{n+1} = \left(1 + \frac{2}{5}x + \frac{1}{20}x^2\right) u^n \tag{72}$$

This leads to a three-stage method including one explicit stage and two implicit ones as follows:

$$\begin{aligned} u^{n+\frac{2}{5}} &= u^n + \frac{2\Delta t}{5} u_t^n + \frac{\Delta t^2}{20} u_{tt}^n \\ \tilde{u} &= u^{n+1} - \frac{\Delta t}{4} u_t^{n+1} + \frac{\Delta t^2}{36} u_{tt}^{n+1} \\ u^{n+1} &= u^{n+\frac{2}{5}} + \frac{3\Delta t}{5} \tilde{u}_t \end{aligned} \tag{73}$$

4.4.4 Sixth-order method

Approximation $R_{3,3}$ in Table 8 which is sixth-order accurate can also be specialized to deal with pure convection problems. The result of the factorization of $R_{3,3}$ in the form

$$\left(1 - \frac{x}{2}(1 - \frac{x}{5} + \frac{x^2}{60})\right) u^{n+1} = \left(1 + \frac{x}{2}(1 + \frac{x}{5} + \frac{x^2}{60})\right) u^n \tag{74}$$

is a four-stage method including two explicit stages and two implicit ones as follows:

$$\begin{aligned} u^{n+\frac{1}{5}} &= u^n + \frac{\Delta t}{5} u_t^n + \frac{\Delta t^2}{60} u_{tt}^n \\ u^{n+\frac{1}{2}} &= u^n + \frac{\Delta t}{2} u_t^{n+\frac{1}{5}} \\ \tilde{u} &= u^{n+1} - \frac{\Delta t}{5} u_t^{n+1} + \frac{\Delta t^2}{60} u_{tt}^{n+1} \\ u^{n+1} &= u^{n+\frac{1}{2}} + \frac{\Delta t}{2} \tilde{u}_t \end{aligned} \tag{75}$$

5 Properties of Padé approximations

In the present Section, the emphasis will be placed on the accuracy and stability properties of the various schemes derived from a multi-stage approach to Padé approximations.

5.1 Stability analysis

To prepare for the analysis of the stability and accuracy properties of the higher-order time integration methods discussed above, we first provide here a brief reminder of the stability definition of numerical schemes for the time integration of initial value problems. This is followed by the analysis of the stability and accuracy properties of selected Padé approximations.

5.1.1 Introduction

The spatial discretization of the advection-diffusion equation leads to the following equations to be solved at each station of the time integration procedure:

$$\frac{\partial \boldsymbol{u}}{\partial t} = \boldsymbol{R}(\boldsymbol{u}) \tag{76}$$

where $\boldsymbol{u}$ is the vector collecting the nodal values of the unknown and $\boldsymbol{R}(\boldsymbol{u})$ stands for the nodal loads arising from the discretization of the first- and second-order spatial operators describing advection and diffusion, respectively.
The time integration of the hybrid hyperbolic-parabolic equations (76) normally proceeds step-by-step starting from given initial values. In truly transient situations, this time-marching process has to be performed in an accurate manner in order to match the actual time evolution of the physical transport problem. On the other hand, for stationary problems only the asymptotic steady solution is relevant. In such cases, the time marching process should be as fast as possible, regardless of its accuracy.
Time integration methods differ from one another by their respective accuracy and stability properties. Due to their conditional stability, the explicit schemes usually lead to severe restrictions on the time-step size so that all error modes arising from truncation errors are not amplified during the time-marching process. On the other hand, an implicit method can be unconditionally stable, which means that all error modes are damped during the time integration, whatever the magnitude of the time step.

5.1.2 Stability criterion

In order to discuss the stability of any time-integration method applied to Eq.(76), we first define the eigenvalues λ of the spatial discretization operator $\boldsymbol{R}$ as [23]

$$\boldsymbol{R}(\boldsymbol{v}) = \lambda \boldsymbol{v} \tag{77}$$

where $\boldsymbol{v}$ is the eigenvector associated to the eigenvalue λ.
If $\boldsymbol{R}(\boldsymbol{u})$ corresponds to the spatially discrete form of a diffusive operator (like the Laplacian $\nabla^2\boldsymbol{u}$), the eigenvalues are purely real and negative, a fact related to the physical dissipative effect. On the other hand, if $\boldsymbol{R}(\boldsymbol{u})$ arises from the discretization of an advection operator (like the gradient $\boldsymbol{\nabla u}$), the eigenvalues are complex with a negative real part if upwinding has been performed in the space discretization. If the discretization of the advective terms is centered, the real part is zero and the eigenvalues are purely imaginary.
The necessary and sufficient stability condition of a time integration method can be derived by a von Neumann analysis, which assumes a linear operator $\boldsymbol{R}$ and a solution $\boldsymbol{u}$ of the form:

$$\boldsymbol{u} = C\exp(\sigma t)\,\boldsymbol{v} \tag{78}$$

where C and σ are complex constants. For example, let us consider the Euler first-order explicit method applied to Eq.(76):

$$\frac{\boldsymbol{u}^{n+1} - \boldsymbol{u}^n}{\Delta t} = \boldsymbol{R}(\boldsymbol{u}^n) \tag{79}$$

Since $\boldsymbol{u}^n = C\,(\exp(\sigma\Delta t))^n\boldsymbol{v}$, we obtain from (77) and (79):

$$\exp(\sigma\Delta t) - 1 = \lambda\Delta t \tag{80}$$

The term $\exp(\sigma\Delta t)$ is the complex amplification factor of Euler method because $\boldsymbol{u}^{n+1}/\boldsymbol{u}^n = \exp(\sigma\Delta t)$. It can be denoted by

$$G = 1 + \lambda\Delta t \tag{81}$$

The stability of the method is ensured if and only if the time step is such that the value of the modulus of the amplification factor is less than unity for all the eigenvalues of the discretization operator $\boldsymbol{R}$. For the example considered, we must have

$$|G|^2 = (1 + \mathrm{Re}(\lambda\Delta t))^2 + (\mathrm{Im}(\lambda\Delta t))^2 \leq 1. \tag{82}$$

This inequality defines the absolute stability region of the Euler explicit method in the $\lambda\Delta t$ complex plane (Fig. 4). The boundary which splits the complex plane into stability and unstability regions corresponds to $|G| = 1$ and is called the *absolute stability curve* of the scheme. For a fixed value of λ, the time step Δt should be sufficiently small so that $\lambda\Delta t$ is located inside the absolute stability region.
In situations where diffusive effects are small with respect to the convective ones, the eigenvalues of $\boldsymbol{R}$ are distributed close to the imaginary axis of the $\lambda\Delta t$ complex plane. A time integration method whose stability region encloses the imaginary axis is then necessary. In the frame of explicit methods, the Euler scheme has therefore to be rejected in favor, for instance, of higher-order explicit Padé approximations or multi-step Runge-Kutta methods which are presented in

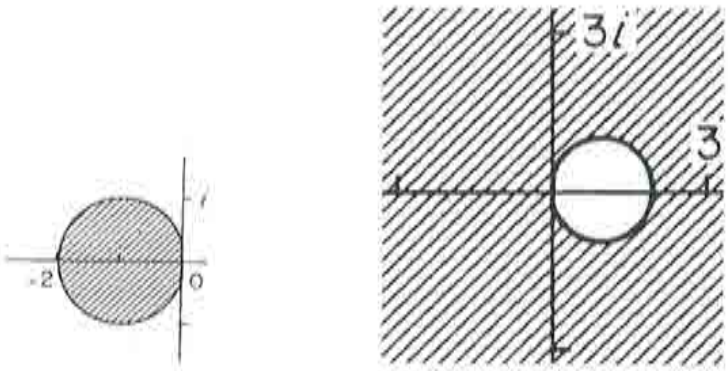

Figure 4: Stability region of forward and backward Euler method.

the next section. However, even if an explicit method has an extended absolute stability region which encloses part of the imaginary axis, the problem of a maximum allowable time step still remains. This is actually the case for all explicit methods.

We have to turn to implicit methods in order to reach unconditional stability. The absolute stability region then encloses the whole left half-plane of the $\lambda\Delta t$ complex plane, including the imaginary axis. As an example, the Euler first-order implicit time scheme applied to Eq.(76) provides

$$\frac{\boldsymbol{u}^{n+1} - \boldsymbol{u}^n}{\Delta t} = \boldsymbol{R}(\boldsymbol{u}^{n+1}) \tag{83}$$

and a stability analysis gives the following expression of the amplification factor:

$$G = \frac{1}{1 - \lambda\Delta t} \tag{84}$$

Its modulus is lower than unity for all complex numbers $\lambda\Delta t$ having a negative real part. The stability curve lies entirely in the right half-plane (Fig. 4). The Euler implicit method is thus unconditionally stable.

As mentioned above, the eigenvalues associated with the convective terms are purely imaginary, while those associated with diffusive terms are real and negative. Hence, an unconditionally stable method whose absolute stability region contains the whole left half (including the imaginary axis) of the $\lambda\Delta t$ complex plane is suitable for applications to advection-diffusion problems. Dahlquist [22] gives the name of A-*stability* to this unconditional stability (without including the imaginary axis). If we accept $|G| = 1$ we can say that by continuity, A-stability is the same as unconditional stability. The Crank-Nicolson scheme is a second order accurate A-stable method. As will be seen later, Padé approximations and the Runge-Kutta methods can provide implicit integration schemes of order higher than two that possess the property of A-stability. Such methods are therefore of great potential interest for a time accurate finite element solution of advection-diffusion problems.

5.1.3 Stability analysis

In order to analyze the stability properties of the various Padé approximations when applied to integrate the first-order initial value problem

$$\begin{aligned} \frac{d\boldsymbol{u}}{dt} &= \boldsymbol{R}(\boldsymbol{u}) \\ \boldsymbol{u}(0) &= \boldsymbol{u}_0 \end{aligned} \tag{85}$$

we follow the von Neumann methodology presented in the previous section and, as before, we define the eigenvalues λ of the spatial discretization operator $\boldsymbol{R}$ as

$$\boldsymbol{R}(\boldsymbol{v}) = \lambda\, \boldsymbol{v} \tag{86}$$

where $\boldsymbol{v}$ is the eigenvector associated to the eigenvalue λ.
To illustrate the application of the von Neumann stability analysis to Padé approximations, we shall consider successively approximation $R_{1,1}$, the Crank-Nicolson method, and approximatiom $R_{2,0}$, which corresponds to the Lax-Wendroff method.
When applied to Eq.(85), approximation $R_{1,1}$ yields, see Eq.(27),

$$\frac{u^{n+1} - u^n}{\Delta t} = \frac{1}{2}\Big(\boldsymbol{R}(\boldsymbol{u}^n) + \boldsymbol{R}(\boldsymbol{u}^{n+1})\Big) \tag{87}$$

Now, according to Eq.(78), one has

$$\begin{aligned} \boldsymbol{u}^n &= C\,(\exp(\sigma\,\Delta t))^n\, \boldsymbol{v} \\ \boldsymbol{u}^{n+1} &= \exp(\sigma \Delta t)\, \boldsymbol{u}^n \end{aligned} \tag{88}$$

and noting that $\exp(\sigma\,\Delta t)$ is the complex amplification factor G, we find from Eqs.(87) and (86) that Padé approximation $R_{1,1}$ possesses the following amplification factor:

$$G\,(R_{1,1}) = \frac{1 + \frac{\lambda \Delta t}{2}}{1 - \frac{\lambda \Delta t}{2}} \tag{89}$$

This relation indicates that the amplification factor of Padé approximation $R_{1,1}$ has the same structure as the approximation itself. We have, by definition of the schemes, the same property for all $R_{n,m}$ methods. It follows that Table 8 contains the amplification factors of all Padé approximations, provided we pose $x = \lambda \Delta t$.
At this point, we can analyze the region of absolute stability of the various Padé approximations using the amplification factors in Table 8. As already mentioned, the stability of a time integration method is ensured if and only if the time step is such that the value of the modulus of the amplification factor is less than unity for all the eigenvalues of the discretization operator $\boldsymbol{R}$. If we admit the unit modulus this leads to the well-known stability condition

$$|G|^2 = [\mathrm{Re}(G)]^2 + [\mathrm{Im}(G)]^2 \leq 1. \tag{90}$$

Some implicit Padé approximations do possess the interesting property of unconditional stability or A-stability. As shown in [9, 10, 17], a Padé approximation $R_{n,m}$ is unconditionally stable if it satisfies the condition:

$$m-2 \leq n \leq m \Longleftrightarrow R_{n,m} \text{ is A} - \text{stable} \tag{91}$$

It follows that the implicit Padé approximations

$$R_{0,1},\ R_{1,1},\ R_{0,2},\ R_{1,2},\ R_{2,2},\ R_{1,3},\ R_{2,3},\ R_{3,3}$$

are A-stable and therefore potentially interesting for the time integration of advection-diffusion equations.

5.2 Phase and damping responses

The phase error Δ and the damping ratio δ_{num}/δ of the implicit A-stable Padé approximations $R_{1,2}, R_{1,3}, R_{2,3}, R_{2,2}$ and $R_{3,3}$ are given in the following Tables for values of the Courant number in the range $0.5 \leq c \leq 4$ and several values of the diffusion number d. The value of the Péclet number $Pe = c/d$ is also indicated in the Tables. Values of $Pe > 1$ indicate that convection dominates the transport process. To appraise the response of the schemes in the limit $Pe \to 0$ and $Pe \to \infty$, we have also produced the phase and damping responses for those limiting cases.
The fully implicit $R_{0,m}$ methods are disregarded because of their poor phase acccuracy.
The phase and damping properties in Tables 9 to 25 have been evaluated using the multi-stage schemes discussed in the previous section assuming a uniform

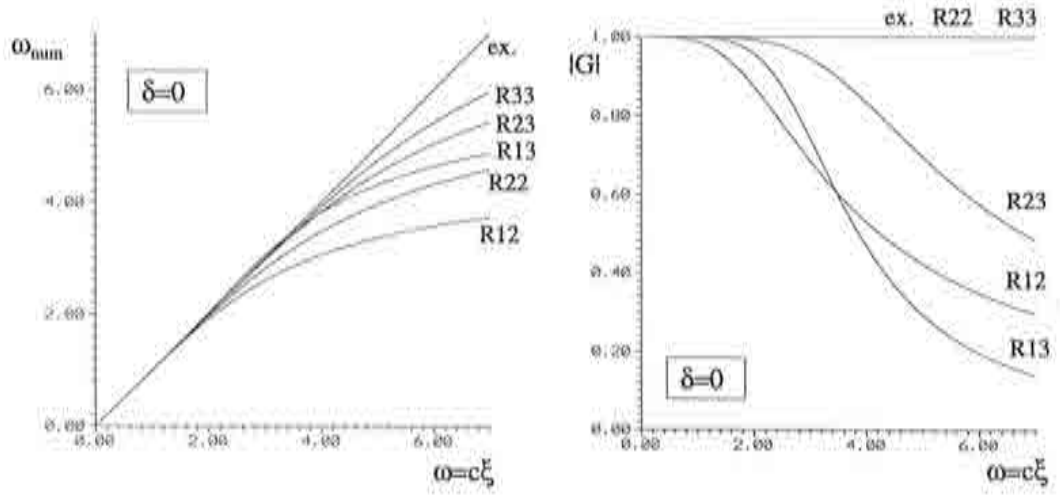

Figure 5: Accuracy of A-stable $R_{n,m}$ methods for pure convection.

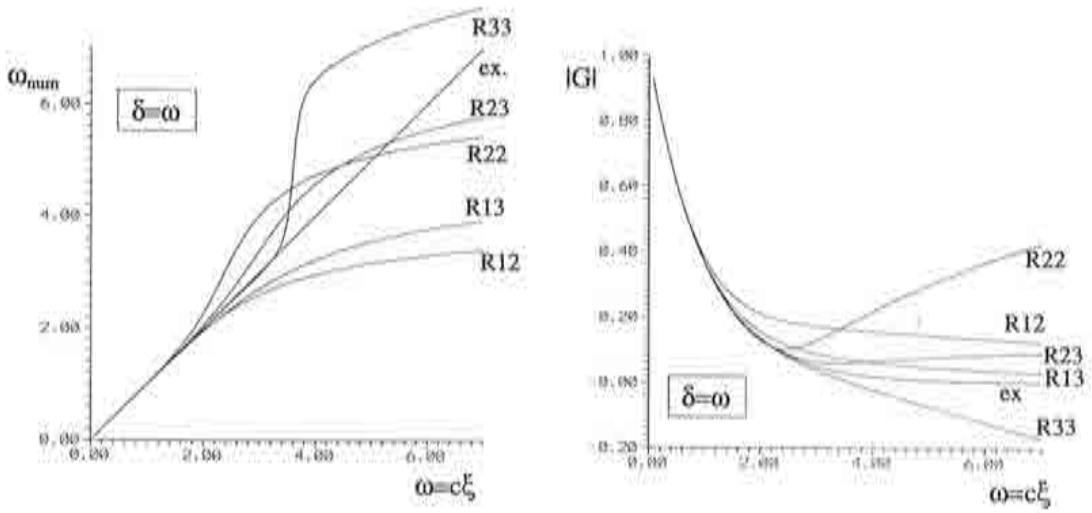

Figure 6: Accuracy of A-stable $R_{n,m}$ methods for convection-diffusion.

mesh of linear finite elements (C^0 interpolations) and using a consistent mass matrix (standard Galerkin method).
Figures 5 to 7 give a graphical representation of the phase and damping responses of the selected implicit Padé schemes. These figures show the response of a Fourier mode e^{ikx} when applied to the linear convection-diffusion Equation (1). Note that the amplification factor of the schemes is given by the simple relationship

$$G(R_{n,m}) = R_{n,m}(\lambda \Delta t). \tag{92}$$

We observe that all methods exibit a good accuracy for diffusion dominated situations (Fig. 7 and Tables 9, 22-25).
On the other hand, several conclusions can be drawn from Figs. 5 and 6 and Tables 10-21.
First of all, we note that scheme $R_{1,2}$ exibits a poor accuracy when the Courant number c exceeds 2. Also scheme $R_{1,3}$ has poor properties for $c > 3$.
Second, we note that, as expected, the $R_{n,n}$ methods are non dissipative and therefore not ideally suited to deal with pure convection problems if centered (Galerkin) approximations are used for the spatial discretization of the convective terms. These methods should therefore be combined with generalized Galerkin (or Petrov-Galerkin) methods for the spatial representation. Unfortunately, such methods like for instance the SUPG method of T.J.R. Hughes [14] include a free parameter which governs the amplitude of the added numerical diffusion. We are currently investigating ways of improving the spatial accuracy of the convective terms without introducing any free parameter and will report on this in a forthcoming publication.
Finally, it should be noted that methods $R_{2,2}$ and $R_{2,3}$ cannot be operated with a Courant number $c > 4$, because of a rather severe accuracy degradation.

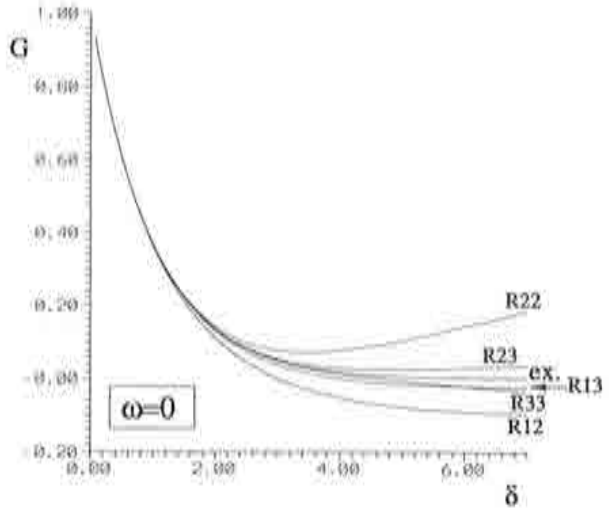

Figure 7: Accuracy of A-stable $R_{n,m}$ methods for pure diffusion.

c	d	Pe	ξ	$R_{1,2}$	$R_{1,3}$	$R_{2,3}$	$R_{2,2}$	$R_{3,3}$
			$\pi/8$	1.0129	1.0129	1.0129	1.0129	1.0129
0	0.05	0	$\pi/4$	1.0524	1.0524	1.0524	1.0524	1.0524
			$\pi/2$	1.2159	1.2159	1.2159	1.2159	1.2159
			$3\pi/4$	1.4281	1.4271	1.4270	1.4270	1.4270
			$\pi/8$	1.0129	1.0129	1.0129	1.0129	1.0129
0	0.1	0	$\pi/4$	1.0524	1.0524	1.0524	1.0524	1.0524
			$\pi/2$	1.2163	1.2159	1.2159	1.2158	1.2159
			$3\pi/4$	1.4354	1.4279	1.4270	1.4262	1.4270
			$\pi/8$	1.0129	1.0129	1.0129	1.0129	1.0129
0	0.2	0	$\pi/4$	1.0524	1.0524	1.0524	1.0524	1.0524
			$\pi/2$	1.2191	1.2161	1.2158	1.2156	1.2159
			$3\pi/4$	1.4925	1.4382	1.4253	1.4127	1.4273

Table 9: Damping ratio δ_{num}/δ

c	d	Pe	ξ	$R_{1,2}$	$R_{1,3}$	$R_{2,3}$	$R_{2,2}$	$R_{3,3}$
			$\pi/8$	-0.0002	-0.0001	-0.0001	-0.0002	-0.0001
1	0	∞	$\pi/4$	-0.0036	-0.0016	-0.0023	-0.0028	-0.0023
			$\pi/2$	-0.0604	-0.0378	-0.0453	-0.0509	-0.0452
			$3\pi/4$	-0.3191	-0.2967	-0.3039	-0.3096	-0.3038
			$\pi/8$	-0.0015	0.0006	-0.0001	-0.0006	-0.0001
2	0	∞	$\pi/4$	-0.0211	0.0064	-0.0026	-0.0094	-0.0024
			$\pi/2$	-0.1720	-0.0284	-0.0561	-0.1051	-0.0498
			$3\pi/4$	-0.4166	-0.2998	-0.3161	-0.3598	-0.3091
			$\pi/8$	-0.0067	0.0032	-0.0002	-0.0026	-0.0002
3	0	∞	$\pi/4$	-0.0726	0.0207	-0.0054	-0.0319	-0.0036
			$\pi/2$	-0.3160	-0.1322	-0.1100	-0.2075	-0.0777
			$3\pi/4$	-0.5273	-0.3949	-0.3679	-0.4445	-0.3377

Table 10: Relative phase error Δ

c	d	Pe	ξ	$R_{1,2}$	$R_{1,3}$	$R_{2,3}$	$R_{2,2}$	$R_{3,3}$
			$\pi/8$	0.9997	1.0000	1.0000	1.0000	1.0000
1	0	∞	$\pi/4$	0.9951	0.9998	1.0000	1.0000	1.0000
			$\pi/2$	0.9481	0.9914	0.9986	1.0000	1.0000
			$3\pi/4$	0.9305	0.9858	0.9977	1.0000	1.0000
			$\pi/8$	0.9951	0.9998	1.0000	1.0000	1.0000
2	0	∞	$\pi/4$	0.9400	0.9890	0.9982	1.0000	1.0000
			$\pi/2$	0.6860	0.7433	0.9465	1.0000	1.0000
			$3\pi/4$	0.6367	0.6600	0.9209	1.0000	1.0000
			$\pi/8$	0.9776	0.9979	0.9997	1.0000	1.0000
3	0	∞	$\pi/4$	0.8096	0.9062	0.9838	1.0000	1.0000
			$\pi/2$	0.4712	0.3685	0.7643	1.0000	1.0000
			$3\pi/4$	0.4297	0.3040	0.7058	1.0000	1.0000

Table 11: Modulus of amplification factor $|G_{num}|$

c	d	Pe	ξ	$R_{1,2}$	$R_{1,3}$	$R_{2,3}$	$R_{2,2}$	$R_{3,3}$
			$\pi/8$	-0.0002	-0.0001	-0.0001	-0.0001	-0.0001
	0.05	10	$\pi/4$	-0.0026	-0.0022	-0.0023	-0.0023	-0.0023
			$\pi/2$	-0.0497	-0.0449	-0.0451	-0.0453	-0.0451
			$3\pi/4$	-0.3101	-0.3044	-0.3037	-0.3032	-0.3036
			$\pi/8$	-0.0002	-0.0001	-0.0001	-0.0001	-0.0001
0.5	0.1	5	$\pi/4$	-0.0029	-0.0022	-0.0023	-0.0023	-0.0023
			$\pi/2$	-0.0517	-0.0455	-0.0451	-0.0449	-0.0451
			$3\pi/4$	-0.3030	-0.3050	-0.3034	-0.3018	-0.3037
			$\pi/8$	-0.0002	-0.0001	-0.0001	-0.0001	-0.0001
	0.2	2.5	$\pi/4$	-0.0032	-0.0023	-0.0023	-0.0023	-0.0023
			$\pi/2$	-0.0490	-0.0465	-0.0450	-0.0437	-0.0451
			$3\pi/4$	-0.2203	-0.2891	-0.3046	-0.3176	-0.3038

Table 12: Relative phase error Δ

c	d	Pe	ξ	$R_{1,2}$	$R_{1,3}$	$R_{2,3}$	$R_{2,2}$	$R_{3,3}$
			$\pi/8$	1.0155	1.0129	1.0129	1.0129	1.0129
	0.05	10	$\pi/4$	1.0620	1.0527	1.0524	1.0522	1.0524
			$\pi/2$	1.2357	1.2197	1.2159	1.2135	1.2158
			$3\pi/4$	1.4155	1.4291	1.4268	1.4246	1.4270
			$\pi/8$	1.0142	1.0129	1.0129	1.0129	1.0129
0.5	0.1	5	$\pi/4$	1.0563	1.0527	1.0524	1.0522	1.0524
			$\pi/2$	1.2133	1.2179	1.2157	1.2141	1.2158
			$3\pi/4$	1.3933	1.4227	1.4270	1.4298	1.4270
			$\pi/8$	1.0135	1.0129	1.0129	1.0129	1.0129
	0.2	2.5	$\pi/4$	1.0530	1.0526	1.0524	1.0523	1.0524
			$\pi/2$	1.1969	1.2146	1.2157	1.2163	1.2159
			$3\pi/4$	1.3919	1.4157	1.4302	1.4479	1.4265

Table 13: Damping ratio δ_{num}/δ

c	d	Pe	ξ	$R_{1,2}$	$R_{1,3}$	$R_{2,3}$	$R_{2,2}$	$R_{3,3}$
			$\pi/8$	-0.0003	-0.0001	-0.0001	-0.0002	-0.0001
	0.05	20	$\pi/4$	-0.0046	-0.0016	-0.0023	-0.0028	-0.0023
			$\pi/2$	-0.0708	-0.0413	-0.0457	-0.0504	-0.0451
			$3\pi/4$	-0.3370	-0.3059	-0.3048	-0.3068	-0.3036
			$\pi/8$	-0.0004	-0.0001	-0.0001	-0.0002	-0.0001
1.0	0.1	10	$\pi/4$	-0.0055	-0.0017	-0.0023	-0.0027	-0.0023
			$\pi/2$	-0.0788	-0.0452	-0.0460	-0.0489	-0.0451
			$3\pi/4$	-0.3420	-0.3142	-0.3041	-0.2986	-0.3034
			$\pi/8$	-0.0005	-0.0001	-0.0001	-0.0002	-0.0001
	0.2	5	$\pi/4$	-0.0072	-0.0020	-0.0023	-0.0026	-0.0023
			$\pi/2$	-0.0872	-0.0529	-0.0459	-0.0432	-0.0449
			$3\pi/4$	-0.3091	-0.3158	-0.2974	-0.2686	-0.3042

Table 14: Relative phase error Δ

c	d	Pe	ξ	$R_{1,2}$	$R_{1,3}$	$R_{2,3}$	$R_{2,2}$	$R_{3,3}$
			$\pi/8$	1.0545	1.0136	1.0130	1.0128	1.0129
	0.05	20	$\pi/4$	1.2021	1.0622	1.0533	1.0498	1.0524
			$\pi/2$	1.5435	1.3154	1.2236	1.1814	1.2150
			$3\pi/4$	1.5039	1.5002	1.4263	1.3749	1.4257
			$\pi/8$	1.0333	1.0134	1.0129	1.0128	1.0129
1.0	0.1	10	$\pi/4$	1.1216	1.0588	1.0528	1.0498	1.0524
			$\pi/2$	1.3148	1.2715	1.2169	1.1828	1.2151
			$3\pi/4$	1.3429	1.4421	1.4201	1.3882	1.4269
			$\pi/8$	1.0226	1.0132	1.0129	1.0128	1.0129
	0.2	5	$\pi/4$	1.0795	1.0569	1.0525	1.0499	1.0524
			$\pi/2$	1.1853	1.2364	1.2127	1.1889	1.2156
			$3\pi/4$	1.2264	1.3769	1.4260	1.4549	1.4296

Table 15: Damping ratio δ_{num}/δ

c	d	Pe	ξ	$R_{1,2}$	$R_{1,3}$	$R_{2,3}$	$R_{2,2}$	$R_{3,3}$
			$\pi/8$	-0.0017	0.0006	-0.0001	-0.0006	-0.0001
	0.05	40	$\pi/4$	-0.0238	0.0056	-0.0027	-0.0094	-0.0024
			$\pi/2$	-0.1838	-0.0462	-0.0597	-0.1044	-0.0496
			$3\pi/4$	-0.4353	-0.3324	-0.3231	-0.3566	-0.3080
			$\pi/8$	-0.0020	0.0006	-0.0001	-0.0006	-0.0001
2.0	0.1	20	$\pi/4$	-0.0263	0.0047	-0.0028	-0.0093	-0.0024
			$\pi/2$	-0.1940	-0.0622	-0.0626	-0.1024	-0.0491
			$3\pi/4$	-0.4478	-0.3570	-0.3256	-0.3466	-0.3046
			$\pi/8$	-0.0024	0.0005	-0.0001	-0.0006	-0.0001
	0.2	10	$\pi/4$	-0.0311	0.0028	-0.0031	-0.0090	-0.0024
			$\pi/2$	-0.2099	-0.0893	-0.0660	-0.0939	-0.0470
			$3\pi/4$	-0.4562	-0.3874	-0.3161	-0.3035	-0.2918

Table 16: Relative phase error Δ

c	d	Pe	ξ	$R_{1,2}$	$R_{1,3}$	$R_{2,3}$	$R_{2,2}$	$R_{3,3}$
			$\pi/8$	1.6437	1.0419	1.0169	1.0104	1.0129
	0.05	40	$\pi/4$	2.9642	1.4461	1.1071	1.0170	1.0514
			$\pi/2$	3.7334	3.5062	1.5696	0.9202	1.1785
			$3\pi/4$	2.3339	2.6482	1.5549	1.0016	1.3614
			$\pi/8$	1.3244	1.0291	1.0149	1.0104	1.0129
2.0	0.1	20	$\pi/4$	1.9590	1.2653	1.0781	1.0171	1.0514
			$\pi/2$	2.2042	2.2855	1.3403	0.9205	1.1793
			$3\pi/4$	1.5159	1.8642	1.3908	1.0006	1.3688
			$\pi/8$	1.1643	1.0227	1.0139	1.0104	1.0129
	0.2	10	$\pi/4$	1.4525	1.1720	1.0632	1.0173	1.0515
			$\pi/2$	1.4353	1.6516	1.2182	0.9215	1.1825
			$3\pi/4$	1.0862	1.4279	1.2972	0.9915	1.4024

Table 17: Damping ratio δ_{num}/δ

c	d	Pe	ξ	$R_{1,2}$	$R_{1,3}$	$R_{2,3}$	$R_{2,2}$	$R_{3,3}$
			$\pi/8$	-0.0072	0.0031	-0.0002	-0.0026	-0.0002
	0.05	60	$\pi/4$	-0.0758	0.0178	-0.0059	-0.0319	-0.0036
			$\pi/2$	-0.3229	-0.1467	-0.1154	-0.2071	-0.0774
			$3\pi/4$	-0.5381	-0.4178	-0.3768	-0.4430	-0.3360
			$\pi/8$	-0.0076	0.0030	-0.0002	-0.0026	-0.0002
3.0	0.1	30	$\pi/4$	-0.0789	0.0150	-0.0064	-0.0318	-0.0036
			$\pi/2$	-0.3293	-0.1601	-0.1200	-0.2060	-0.0764
			$3\pi/4$	-0.5468	-0.4373	-0.3821	-0.4386	-0.3310
			$\pi/8$	-0.0085	0.0029	-0.0002	-0.0026	-0.0002
	0.2	15	$\pi/4$	-0.0847	0.0095	-0.0073	-0.0313	-0.0035
			$\pi/2$	-0.3404	-0.1842	-0.1267	-0.2017	-0.0724
			$3\pi/4$	-0.5584	-0.4667	-0.3826	-0.4214	-0.3096

Table 18: Relative phase error Δ

c	d	Pe	ξ	$R_{1,2}$	$R_{1,3}$	$R_{2,3}$	$R_{2,2}$	$R_{3,3}$
			$\pi/8$	3.9176	1.3042	1.0567	1.0009	1.0127
	0.05	60	$\pi/4$	7.6109	4.2928	1.5608	0.9190	1.0432
			$\pi/2$	6.4702	8.6884	3.0120	0.5901	1.0018
			$3\pi/4$	3.4202	4.8869	2.1241	0.6054	1.0902
			$\pi/8$	2.4484	1.1660	1.0345	1.0009	1.0127
3.0	0.1	30	$\pi/4$	4.1857	2.6907	1.2943	0.9190	1.0432
			$\pi/2$	3.4228	4.6463	1.9198	0.5895	1.0023
			$3\pi/4$	1.9038	2.7519	1.4907	0.6002	1.0918
			$\pi/8$	1.7130	1.0966	1.0234	1.0009	1.0127
	0.2	15	$\pi/4$	2.4709	1.8827	1.1596	0.9192	1.0433
			$\pi/2$	1.9015	2.6281	1.3693	0.5868	1.0042
			$3\pi/4$	1.1447	1.6857	1.1598	0.5784	1.0970

Table 19: Damping ratio δ_{num}/δ

c	d	Pe	ξ	$R_{1,2}$	$R_{1,3}$	$R_{2,3}$	$R_{2,2}$	$R_{3,3}$
			$\pi/8$	-0.0198	0.0084	-0.0005	-0.0074	-0.0003
	0.05	80	$\pi/4$	-0.1515	0.0059	-0.0175	-0.0733	-0.0085
			$\pi/2$	-0.4353	-0.2707	-0.2030	-0.3127	-0.1374
			$3\pi/4$	-0.6173	-0.5067	-0.4475	-0.5243	-0.3902
			$\pi/8$	-0.0204	0.0082	-0.0005	-0.0074	-0.0003
4	0.1	40	$\pi/4$	-0.1541	0.0017	-0.0185	-0.0732	-0.0085
			$\pi/2$	-0.4392	-0.2790	-0.2067	-0.3122	-0.1366
			$3\pi/4$	-0.6229	-0.5191	-0.4522	-0.5225	-0.3870
			$\pi/8$	-0.0217	0.0078	-0.0006	-0.0073	-0.0003
	0.2	20	$\pi/4$	-0.1591	-0.0064	-0.0202	-0.0728	-0.0084
			$\pi/2$	-0.4463	-0.2947	-0.2128	-0.3103	-0.1336
			$3\pi/4$	-0.6319	-0.5400	-0.4567	-0.5156	-0.3743

Table 20: Relative phase error Δ

c	d	Pe	ξ	$R_{1,2}$	$R_{1,3}$	$R_{2,3}$	$R_{2,2}$	$R_{3,3}$
			$\pi/8$	9.0025	2.4971	1.2426	0.9786	1.0120
	0.05	80	$\pi/4$	13.930	12.323	3.1410	0.7690	1.0121
			$\pi/2$	8.7497	13.529	5.0319	0.3740	0.7353
			$3\pi/4$	4.3550	6.9183	2.9065	0.3738	0.7546
			$\pi/8$	4.9629	1.7728	1.1266	0.9786	1.0120
4	0.1	40	$\pi/4$	7.2427	6.6208	2.0499	0.7690	1.0121
			$\pi/2$	4.4881	6.9384	2.7898	0.3735	0.7350
			$3\pi/4$	2.2945	3.6402	1.7301	0.3708	0.7514
			$\pi/8$	2.9422	1.4099	1.0684	0.9786	1.0120
	0.2	20	$\pi/4$	3.8990	3.7649	1.5023	0.7690	1.0122
			$\pi/2$	2.3600	3.6490	1.6692	0.3717	.07338
			$3\pi/4$	1.2677	2.0119	1.1377	0.3592	.07376

Table 21: Damping ratio δ_{num}/δ

c	d	Pe	ξ	$R_{1,2}$	$R_{1,3}$	$R_{2,3}$	$R_{2,2}$	$R_{3,3}$
			$\pi/8$	-0.0001	-0.0001	-0.0001	-0.0001	-0.0001
0.025	0.05	0.5	$\pi/4$	-0.0023	-0.0023	-0.0023	-0.0023	-0.0023
			$\pi/2$	-0.0449	-0.0451	-0.0451	-0.0451	-0.0451
			$3\pi/4$	-0.3015	-0.3035	-0.3036	-0.3038	-0.3036
			$\pi/8$	-0.0001	-0.0001	-0.0001	-0.0001	-0.0001
0.05	0.1	0.5	$\pi/4$	-0.0023	-0.0023	-0.0023	-0.0023	-0.0023
			$\pi/2$	-0.0438	-0.0450	-0.0451	-0.0451	-0.0451
			$3\pi/4$	-0.2878	-0.3017	-0.3038	-0.3056	-0.3036
			$\pi/8$	-0.0001	-0.0001	-0.0001	-0.0001	-0.0001
0.1	0.2	0.5	$\pi/4$	-0.0022	-0.0023	-0.0023	-0.0023	-0.0023
			$\pi/2$	-0.0358	-0.0442	-0.0451	-0.0458	-0.0451
			$3\pi/4$	-0.1741	-0.2787	-0.3084	-0.3392	-0.3028

Table 22: Relative phase error Δ

c	d	Pe	ξ	$R_{1,2}$	$R_{1,3}$	$R_{2,3}$	$R_{2,2}$	$R_{3,3}$
			$\pi/8$	1.0129	1.0129	1.0129	1.0129	1.0129
0.025	0.05	0.5	$\pi/4$	1.0524	1.0524	1.0524	1.0524	1.0524
			$\pi/2$	1.2159	1.2159	1.2159	1.2159	1.2159
			$3\pi/4$	1.4281	1.4271	1.4270	1.4270	1.4270
			$\pi/8$	1.0129	1.0129	1.0129	1.0129	1.0129
0.05	0.1	0.5	$\pi/4$	1.0524	1.0524	1.0524	1.0524	1.0524
			$\pi/2$	1.2161	1.2159	1.2159	1.2158	1.2159
			$3\pi/4$	1.4349	1.4278	1.4270	1.4263	1.4270
			$\pi/8$	1.0129	1.0129	1.0129	1.0129	1.0129
0.1	0.2	0.5	$\pi/4$	1.0524	1.0524	1.0524	1.0524	1.0524
			$\pi/2$	1.2179	1.2160	1.2159	1.2158	1.2159
			$3\pi/4$	1.4877	1.4372	1.4256	1.4144	1.4272

Table 23: Damping ratio δ_{num}/δ

c	d	Pe	ξ	$R_{1,2}$	$R_{1,3}$	$R_{2,3}$	$R_{2,2}$	$R_{3,3}$
			$\pi/8$	-0.0001	-0.0001	-0.0001	-0.0001	-0.0001
0.005	0.05	0.1	$\pi/4$	-0.0023	-0.0023	-0.0023	-0.0023	-0.0023
			$\pi/2$	-0.0449	-0.0451	-0.0451	-0.0451	-0.0451
			$3\pi/4$	-0.3015	-0.3035	-0.3036	-0.3038	-0.3036
			$\pi/8$	-0.0001	-0.0001	-0.0001	-0.0001	-0.0001
0.01	0.1	0.1	$\pi/4$	-0.0023	-0.0023	-0.0023	-0.0023	-0.0023
			$\pi/2$	-0.0438	-0.0450	-0.0451	-0.0451	-0.0451
			$3\pi/4$	-0.2876	-0.3016	-0.3038	-0.3056	-0.3036
			$\pi/8$	-0.0001	-0.0001	-0.0001	-0.0001	-0.0001
0.02	0.2	0.1	$\pi/4$	-0.0022	-0.0023	-0.0023	-0.0023	-0.0023
			$\pi/2$	-0.0353	-0.0441	-0.0451	-0.0460	-0.0451
			$3\pi/4$	-0.1719	-0.2783	-0.3086	-0.3401	-0.3028

Table 24: Relative phase error Δ

c	d	Pe	ξ	$R_{1,2}$	$R_{1,3}$	$R_{2,3}$	$R_{2,2}$	$R_{3,3}$
			$\pi/8$	1.0129	1.0129	1.0129	1.0129	1.0129
0.005	0.05	0.1	$\pi/4$	1.0524	1.0524	1.0524	1.0524	1.0524
			$\pi/2$	1.2159	1.2159	1.2159	1.2159	1.2159
			$3\pi/4$	1.4281	1.4271	1.4270	1.4270	1.4270
			$\pi/8$	1.0129	1.0129	1.0129	1.0129	1.0129
0.01	0.1	0.1	$\pi/4$	1.0524	1.0524	1.0524	1.0524	1.0524
			$\pi/2$	1.2163	1.2159	1.2159	1.2158	1.2159
			$3\pi/4$	1.4354	1.4279	1.4270	1.4262	1.4270
			$\pi/8$	1.0129	1.0129	1.0129	1.0129	1.0129
0.02	0.2	0.1	$\pi/4$	1.0524	1.0524	1.0524	1.0524	1.0524
			$\pi/2$	1.2190	1.2161	1.2158	1.2156	1.2159
			$3\pi/4$	1.4924	1.4381	1.4253	1.4128	1.4273

Table 25: Damping ratio δ_{num}/δ

6 Runge-Kutta and Padé methods. Relations

The Runge-Kutta methods are multi-stage methods that only make use of the solution u^n at time t^n to compute the next solution u^{n+1}. This is achieved by computing a number k of intermediate values of the time derivative of the unknown u, within the interval $\Delta t = t^{n+1} - t^n$. Applied to the differential equation

$$\frac{du}{dt} = R(u,t) \tag{93}$$

the most general form of a k-stage Runge-Kutta method is written as follows [9, 17, 21]:

$$\delta_i = \Delta t\, R\left(u^n + \sum_{j=1}^{k} a_{ij}\,\delta_j\,,\, t^n + c_i \Delta t\right) \qquad i = 1, \cdots, k \tag{94}$$

$$u^{n+1} = u^n + \sum_{i=1}^{k} b_i\,\delta_i \tag{95}$$

The associated consistency conditions are (see e.g. [9])

$$c_i = \sum_{j=1}^{k} a_{ij} \quad \text{and} \quad \sum_{i=1}^{k} b_i = 1 \tag{96}$$

The widely used explicit Runge-Kutta methods are such that $a_{ij} = 0$ for $j \geq i$. Some of them are recalled in the next section. If this condition is not satisfied, the methods are implicit. Some implicit Runge-Kutta methods will be presented in subsequent sub-sections. Despite their complexity, such methods appear to be of great interest due to their accuracy and stability properties.
As we have seen in section 5.1.2, we need to study the test equation $dy/dt = \lambda y$ where $y = y(t)$ and $\lambda \in \boldsymbol{C}$ to take into account the stability and accuracy properties. We can compute the amplification factor G from there. G is a function of $z = \lambda \Delta t$ defined by $R(z) = P(z)/Q(z)$ where $P(z)$ and $Q(z)$ are polinomials. $R(z)$ is called the stability function and $S = \{z \in \boldsymbol{C};\, |R(z)| \leq 1\}$ the stability domain. Using this notation we can say that the numerical method is A-stable if and only if $S \supset \{z \in \boldsymbol{C} \,|\, \mathrm{Re}(z) \leq 0\}$. There is a necessary and sufficient condition for A-stability which is obtained from the maximum principle applied to $\boldsymbol{C}^-$ [10].

$$\left.\begin{array}{r} R(z) \text{ analytic for } \mathrm{Re}(z) < 0 \\ |R(\alpha i)| \leq 1 \quad \forall \alpha \in \boldsymbol{R} \end{array}\right\} \Leftrightarrow \quad \text{A-stable} \tag{97}$$

It is shown in [10] that if the temporal order of a numerical method is n, then $R(z)$ is an approximation of order n to the exponential, i.e. $e^z - R(z) = O(z^{n+1})$. The reciprocal relation is also true if n is the maximum integer that verifies the last relation.

6.1 Explicit Runge-Kutta methods

The most simple explicit Runge-Kutta method is the second-order two-stage method:

$$\begin{aligned} \delta_1 &= \Delta t\, R(u^n, t^n) \\ \delta_2 &= \Delta t\, R\left(u^n + \tfrac{1}{2}\delta_1, t^n + \tfrac{1}{2}\Delta t\right) \\ u^{n+1} &= u^n + \frac{1}{2}(\delta_1 + \delta_2) \end{aligned} \tag{98}$$

This method is unfortunately not adapted to deal with convection dominated problems, because, as shown in Fig. 8, the associated stability region does not include any portion of the imaginary axis. This method has the same stability function that the multistage $R_{2,0}$ Padé approximation.
The most popular explicit Runge-Kutta method is the classical fourth-order four stage scheme:

$$\begin{aligned} \delta_1 &= \Delta t\, R(u^n, t^n) \\ \delta_2 &= \Delta t\, R\left(u^n + \tfrac{1}{2}\delta_1, t^n + \tfrac{1}{2}\Delta t\right) \\ \delta_3 &= \Delta t\, R\left(u^n + \tfrac{1}{2}\delta_2, t^n + \tfrac{1}{2}\Delta t\right) \\ \delta_4 &= \Delta t\, R(u^n + \delta_3, t^n + \Delta t) \\ u^{n+1} &= u^n + \frac{1}{6}(\delta_1 + 2\delta_2 + 2\delta_3 + \delta_4) \end{aligned} \tag{99}$$

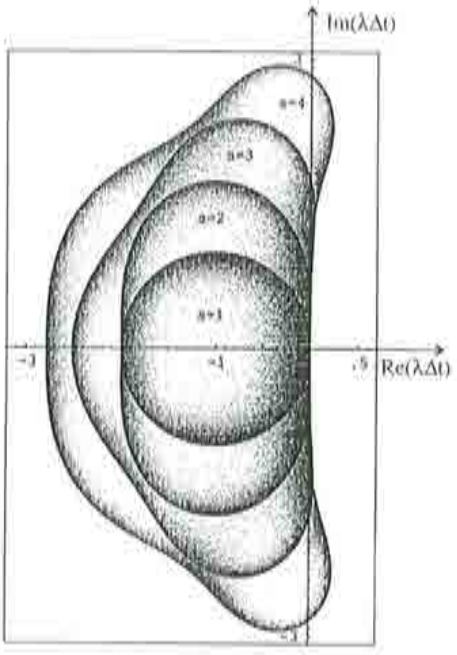

Figure 8: Stability region of explicit Padé and Runge-Kutta methods of order s.

As shown in [13], the amplification factor of the above fourth-order Runge-Kutta method is given by:

$$G = 1 + (\lambda\Delta t) + \frac{1}{2!}(\lambda\Delta t)^2 + \frac{1}{3!}(\lambda\Delta t)^3 + \frac{1}{4!}(\lambda\Delta t)^4 \qquad (100)$$

The method is effectively fourth-order accurate since G matches $\exp(\lambda\Delta t)$ to the fourth-order term. The associated absolute stability curve is the same as that of Padé approximation $R_{0,4}$ and is shown in Fig. 8. It cuts the real and imaginary axes at -2.78 and $\pm 2\sqrt{2}$, respectively [13]. Since the absolute stability region contains a finite portion of the imaginary axis, the method can be used in convection dominated situations.

6.2 Similarities between explicit Runge-Kutta and Padé methods

In the explicit algorithms like $R_{n,0}$ or explicit Runge-Kutta $R(z)$ is a polinomial, that is, $Q(z) = 1$. From there we can deduce that any explicit method can not be A-stable because $\deg(Q) < \deg(P)$. The stability function of an n order explicit method is

$$R(z) = 1 + \frac{z}{1!} + \frac{z^2}{2!} + \cdots + \frac{z^n}{n!} + T(z) \quad \text{where } T(z) = O(z^{n+1})$$

that is,

$$R(z) = R_{n,0}(z) + T(z) \quad \text{where } T(z) = O(z^{n+1}) \qquad (101)$$

In the multistage Taylor-Galerkin methods (explicit multistage Padé methods) we obtain that $T(z) = 0$ (see section 5.1). We have the same property in the explicit n-order n-stages Runge-Kutta methods [10]. We can conclude that the multistage Taylor-Galerkin and the n-stages n-order Runge-Kutta methods are equivalent for linear problems. The difference resides only on the implementation. We must remember that the maximum order of a n-stage n-order Runge-Kutta method is 4.

6.3 Classical implicit Runge-Kutta methods

Generally, the application of an implicit Runge-Kutta method requires the simultaneous solution of the k equations for the increments δ_i $(i = 1, \cdots, k)$. Each of these increments is a nonlinear function of all the δ_j $(j = 1, \cdots, k)$.
An example of a two-stage implicit Runge-Kutta method is given by

$$\begin{aligned} \delta_1 &= \Delta t\, R(u^n) \\ \delta_2 &= \Delta t\, R\left(u^n + \frac{1}{2}\delta_1 + \frac{1}{2}\delta_2\right) \\ u^{n+1} &= u^n + \frac{1}{2}\delta_1 + \frac{1}{2}\delta_2 \end{aligned} \qquad (102)$$

which is of course the trapezoidal rule. The method is of order two and A-stable. Butcher (see e.g. [9]) has deeply investigated k-stage Runge-Kutta methods and shown that, for each value of k, there is one method of order $2k$. Moreover, Crouzeix [2] has demonstrated that such high-order methods are A-stable. This is indeed a very attractive property of implicit Runge-Kutta methods in view of their application in the solution of transient advection-diffusion problems. This kind of methods are the Gauss methods. There are other classical families of implicit Runge-Kutta methods. They are the Radau-IA and Radau-IIA k-stage of order $2k-1$, and the Lobatto-IIIA, Lobatto-IIIB and Lobatto IIIC k-stage of order $2k-2$ [9, 17].
The only fourth-order accurate two-stage implicit Runge-Kutta method is given by [17]

$$[a_{ij}] = \begin{bmatrix} \frac{1}{4} & \frac{1}{4} - \frac{\sqrt{3}}{6} \\ \frac{1}{4} + \frac{\sqrt{3}}{6} & \frac{1}{4} \end{bmatrix} \quad b = \begin{pmatrix} \frac{1}{2} \\ \frac{1}{2} \end{pmatrix} \quad c = \begin{pmatrix} \frac{1}{2} - \frac{\sqrt{3}}{6} \\ \frac{1}{2} + \frac{\sqrt{3}}{6} \end{pmatrix} \tag{103}$$

The method then reads

$$\begin{aligned} \delta_1 &= \Delta t\, R(u^n + a_{11}\delta_1 + a_{12}\delta_2\,,\, t^n + c_1\Delta t) \\ \delta_2 &= \Delta t\, R(u^n + a_{21}\delta_1 + a_{22}\delta_2\,,\, t^n + c_2\Delta t) \\ u^{n+1} &= u^n + b_1\delta_1 + b_2\delta_2 \end{aligned} \tag{104}$$

The size of the implicit system associated with this method is double when compared to standard second-order methods, since δ_1 and δ_2 must be simultaneously determined. This is the price to pay to obtain an unconditionally stable fourth-order accurate time integration scheme. To solve such set of nonlinear equations, a Newton-Raphson iterative process should be applied. We can not use a fixed-point iteration, it transforms the algorithm into an explicit method and destroys the good stability properties [10].

6.4 Similarities between classical implicit Runge-Kutta and Padé methods

As in 6.2, we can say that two methods are equivalent if they have the same stability function. You can see this relations in Table 26 (see Section 5.1 and [17]). The phase and damping properties of these schemes have been studied in Section 5.
The extensions of Simpson quadrature rule (see Section 7) have n steps and order $2n$. So, the stability function $P(z)/Q(z)$ is a $2n$-order approximation to the exponential function with $\deg(P) \leq n$ and $\deg(Q) \leq n$. The Padé approximation $R_{n,n}(z)$ is the unique rational function with these properties. Therefore their stability function is $R_{n,n}(z)$. This family is equivalent to the multistage Padé schemes $R_{n,n}$ and the gaussian implicit Runge-Kutta methods, and they have the same stability and accuracy properties.

Implicit RK method	multistage Padé method	order	stability function
Gauss	$R_{n,n}$	$2n$	$R_{n,n}(z)$
Radau IA	$R_{n-1,n}$	$2n-1$	$R_{n-1,n}(z)$
Radau IIA	$R_{n-1,n}$	$2n-1$	$R_{n-1,n}(z)$
Lobatto IIIA	$R_{n-1,n-1}$	$2n-2$	$R_{n-1,n-1}(z)$
Lobatto IIIB	$R_{n-1,n-1}$	$2n-2$	$R_{n-1,n-1}(z)$
Lobatto IIIC	$R_{n-2,n}$	$2n-2$	$R_{n-2,n}(z)$

Table 26: Relations between the implicit Runge-Kutta methods and the Padé schemes.

6.5 Other implicit Runge-Kutta methods

Among the variety of implicit Runge-Kutta methods, there is an interesting family of schemes in view of its diagonally implicit character (DIRK method). The matrix A that defines these methods is lower triangular, that is, $a_{ij} = 0$ if $i < j$. The great advantage of this family of methods is indeed the absence of coupling between two stages which reduces the size of the systems to be solved at each step of the time integration procedure. This is a nice computational feature. The stability function of a DIRK method is then defined by

$$R(z) = \frac{P(z)}{(1 - a_{11}z)(1 - a_{22}z)\cdots(1 - a_{ss}z)} \tag{105}$$

where s is the number of stages. Notice that $Q(z) = \det(I - z\,A)$, where I is the identity matrix.
A known DIRK method is the one defined by [23]

$$[a_{ij}] = \begin{bmatrix} 1 & 0 \\ -\frac{1}{3} & \frac{2}{3} \end{bmatrix} \quad b = \begin{pmatrix} \frac{1}{4} \\ \frac{3}{4} \end{pmatrix} \quad c = \begin{pmatrix} 1 \\ \frac{1}{3} \end{pmatrix} \tag{106}$$

With the above parameters, the two-step third-order method reads:

$$\begin{aligned} \delta_1 &= \Delta t\, R(u^n + \delta_1\,,\, t^n + \Delta t) \\ \delta_2 &= \Delta t\, R\left(u^n - \frac{1}{3}\delta_1 + \frac{2}{3}\delta_2\,,\, t^n + \frac{1}{3}\Delta t\right) \\ u^{n+1} &= u^n + \frac{1}{4}\delta_1 + \frac{3}{4}\delta_2 \end{aligned} \tag{107}$$

While the above third order method works well for pure convection, its behaviour in mixed advection-diffusion situations is generally disappointing. (See Tables 27-28, Figs. 9-11 and references [10, 23, 27]).
Similarly to other DIRK methods the previous one has to solve two uncoupled systems at each time step. By contrast, the two-stage fourth-order method in

ξ	c	d	Pe	DIRK	c	d	Pe	DIRK	c	d	Pe	DIRK
$\pi/8$				-0.0044				-0.0069				-0.0190
$\pi/4$	0.5	0.0	∞	-0.0187	0.5	0.05	10	-0.0283	1.0	0.05	20	-0.0695
$\pi/2$				-0.0977				-0.1292				-0.2219
$3\pi/4$				-0.3486				-0.3943				-0.4586
$\pi/8$				-0.0166				-0.0094				-0.0214
$\pi/4$	1.0	0.0	∞	-0.0617	0.5	0.1	5	-0.0374	1.0	0.1	10	-0.0767
$\pi/2$				-0.2048				-0.1524				-0.2349
$3\pi/4$				-0.4353				-0.4063				-0.4651
$\pi/8$				-0.0600				-0.0143				-0.0259
$\pi/4$	2.0	0.0	∞	-0.1796	0.5	0.2	2.5	-0.0538	1.0	0.2	5	-0.0900
$\pi/2$				-0.3976				-0.1776				-0.2495
$3\pi/4$				-0.5815				-0.3335				-0.4280

Table 27: Phase errors Δ of DIRK method.

ξ	c	d	Pe	DIRK	c	d	Pe	DIRK	c	d	Pe	DIRK
$\pi/8$				0.9937				1.8232				4.1591
$\pi/4$	0.5	0.0	∞	0.9758	0.5	0.05	10	1.7932	1.0	0.05	20	3.7197
$\pi/2$				0.9220				1.6781				2.6386
$3\pi/4$				0.9096				1.4930				1.7589
$\pi/8$				0.9757				1.4098				2.5600
$\pi/4$	1.0	0.0	∞	0.9161	0.5	0.1	5	1.3911	1.0	0.1	10	2.2969
$\pi/2$				0.7906				1.3397				1.6895
$3\pi/4$				0.7691				1.3082				1.2927
$\pi/8$				0.9158				1.2013				1.7590
$\pi/4$	2.0	0.0	∞	0.7801	0.5	0.2	2.5	1.1844	1.0	0.2	5	1.5829
$\pi/2$				0.6325				1.1612				1.2176
$3\pi/4$				0.6161				1.2261				1.0544

Table 28: Damping ratios δ_{num}/δ of DIRK method. For $Pe = \infty$ the modulus of the amplification factor $|G|$.

Eq.(103) leads to fully coupled equations and the size of the associated linear system in the Newton-Raphson iterative solution process is doubled with respect to this third-order method.
We consider now some more general families of DIRK methods. For example, the two stage methods defined by

$$A = \begin{pmatrix} \frac{3\mu-1}{6\mu} & 0 \\ \mu & \frac{1-\mu}{2} \end{pmatrix} \quad b = \begin{pmatrix} \frac{3\mu^2}{3\mu^2+1} \\ \frac{1}{3\mu^2+1} \end{pmatrix} \quad c = \begin{pmatrix} \frac{3\mu-1}{6\mu} \\ \frac{1+\mu}{2} \end{pmatrix} \tag{108}$$

have third order and are A-stables if $\mu = -1/\sqrt{3}$ ($DIRK(1)$ method) and if $\mu = -1/3$ (Eq.(106), $DIRK(2)$ method).
If all the diagonal terms of the matrix A are the same, it is a singly diagonally implicit Runge-Kutta method (SDIRK). A family of two stage SDIRK methods is given by

$$A = \begin{pmatrix} \mu & 0 \\ 1-2\mu & \mu \end{pmatrix} \quad b = \begin{pmatrix} \frac{1}{2} \\ \frac{1}{2} \end{pmatrix} \quad c = \begin{pmatrix} \mu \\ 1-\mu \end{pmatrix}. \tag{109}$$

If $\mu = (3+\sqrt{3})/6$ it has third order and is A-stable ($SDIRK(1)$ method), and if $\mu = (2-\sqrt{2})/2$ it has second order and is A-stable ($SDIRK(2)$ method). The three stage SDIRK family defined by

$$A = \begin{pmatrix} \frac{1+\mu}{2} & 0 & 0 \\ -\frac{\mu}{2} & \frac{1+\mu}{2} & 0 \\ 1+\mu & -1-2\mu & \frac{1+\mu}{2} \end{pmatrix} \quad b = \begin{pmatrix} \frac{1}{6\mu^2} \\ 1-\frac{1}{3\mu^2} \\ \frac{1}{6\mu^2} \end{pmatrix} \quad c = \begin{pmatrix} \frac{1+\mu}{2} \\ \frac{1}{2} \\ \frac{1-\mu}{2} \end{pmatrix} \tag{110}$$

has fourth order if $3\mu^3 - 3\mu - 1 = 0$, but it is fourth order A-stable only if $\mu = 2\cos(\pi/18)/\sqrt{3}$ ($SDIRK(3)$ method).
There is another family of Runge-Kutta methods called singly implicit Runge-Kutta methods (SIRK). In this case you can diagonalize the matrix A, and it has only one eigenvalue. A two stage SIRK method is defined by

$$A = \begin{pmatrix} \frac{1}{4}\mu(4-\sqrt{2}) & \frac{1}{4}\mu(4-3\sqrt{2}) \\ \frac{1}{4}\mu(4+3\sqrt{2}) & \frac{1}{4}\mu(4-\sqrt{2}) \end{pmatrix} \; b = \begin{pmatrix} \frac{4\mu(1+\sqrt{2})-\sqrt{2}}{8\mu} \\ \frac{4\mu(1-\sqrt{2})+\sqrt{2}}{8\mu} \end{pmatrix} \; c = \begin{pmatrix} (2-\sqrt{2})\mu \\ (2+\sqrt{2})\mu \end{pmatrix} \tag{111}$$

It is third order A-stable if $\mu = (3+\sqrt{3})/6$ ($SIRK$ method).
There is a big variety of DIRK, SDIRK and SIRK methods. These schemes increase the number of stages but not the order. This generally diminishes some of its atractive properties.
The methods $DIRK(1)$, $SDIRK(1)$, and $SIRK$ are equivalents, because they have the same stability function. The stability functions of DIRK schemes are in Table 29. The main difference between Table 29 and 26 is that the poles of the stability function in Table 26 are pure complex, and those of Table 29 are real. It makes the possibility to be uncoupled the DIRK, SDIRK and SIRK schemes and to solve them more easily.

method	stability function
DIRK(1)	$\frac{1-\frac{1}{\sqrt{3}}z-\frac{1+\sqrt{3}}{6}z^2}{1-\left(1+\frac{1}{\sqrt{3}}\right)z+\left(\frac{2+\sqrt{3}}{6}\right)z^2}$
DIRK(2)	$\frac{1-\frac{2}{3}z-\frac{1}{2}z^2}{1-\frac{5}{3}z+\frac{2}{3}z^2}$
SDIRK(2)	$\frac{1+(\sqrt{2}-1)z}{1-\left(2-\sqrt{2}\right)z+\left(\frac{3}{2}-\sqrt{2}\right)z^2}$
SDIRK(3)	$\frac{-24\mu+(36\mu^2+12\mu)z+(6\mu-18\mu^3)z^2+(3\mu^4-3\mu^3-9\mu^2-7\mu-2)z^3}{3\mu(-8+(12+12\mu)z-(6+12\mu+6\mu^2)z^2+(3\mu+3\mu^2+\mu^3+1)z^3)}$

Table 29: Stability functions of DIRK methods $\left(\mu=\frac{2}{\sqrt{3}}\cos\left(\frac{\pi}{18}\right)\right)$.

There is a more general feature. Let $R(z)=P(z)/Q(z)$ an irreducible A-stable polinomial quotient satisfying $P(0)=Q(0)=1$, $\mathrm{gr}(P)\leq\mathrm{gr}(Q)=s$ and $e^z-R(z)=O(z^{n+1})$. Then there exists an s-stage A-stable n-order Runge-Kutta method with $R(z)$ as stability function [10]. So, it is possible to find as many A-stable Runge-Kutta methods as irreducible A-stable polinomial quotients.

6.6 Similarities between non classical implicit Runge-Kutta and Padé methods

We extend here the multistage Padé methods. If we take an irreducible A-stable polinomial quotient $R(z)=P(z)/Q(z)$ satisfying $R(z)-e^z=O(z^{n+1})$. Then there exists an s-stage n-order multistage method where $s\leq\deg(Q)+\deg(P)$ (like Padé methods) with $R(z)$ as stability function. We will call these methods as A-stable exponential methods.

For instance, the function

$$R(z)=\frac{1-\frac{2}{3}z-\frac{1}{2}z^2}{1-\frac{5}{3}z+\frac{2}{3}z^2} \tag{112}$$

is an aproximation to the exponential function of order 3. It corresponds to the stability function of the DIRK method defined in Equation (106). We can factor like

$$R(z)=\frac{\left(1-\frac{3}{-2+\sqrt{22}}z\right)\left(1-\frac{3}{-2-\sqrt{22}}z\right)}{(1-z)(1-\frac{2}{3}z)} \tag{113}$$

This factorization allows us to write the following exponential method

$$\begin{aligned} \left(1-\tfrac{2}{3}x\right)\tilde{u} &= \left(1-\tfrac{3}{-2-\sqrt{22}}x\right)u^n \\ (1-x)\,u^{n+1} &= \left(1-\tfrac{3}{-2+\sqrt{22}}x\right)\tilde{u} \end{aligned} \tag{114}$$

where $x = \Delta t\,\frac{\partial}{\partial t}$. There are two uncoupled implicit equations to solve at each time step. We can also factor in another way

$$R(z) = \frac{1}{1-\frac{2}{3}z}\,\frac{1-\frac{2}{3}z\left(1+\frac{3}{4}z\right)}{1-z} \tag{115}$$

giving an equivalent method. By this factorization the exponential method reads

$$\begin{aligned} u^{n+\frac{3}{4}} &= \left(1+\tfrac{3}{4}x\right)u^n \\ (1-x)\,\tilde{u} &= \left(1-\tfrac{2}{3}x\right)u^{n+\frac{3}{4}} \\ \left(1-\tfrac{2}{3}x\right)u^{n+1} &= \tilde{u} \end{aligned} \tag{116}$$

There are more possibilities, but all of them are equivalent.

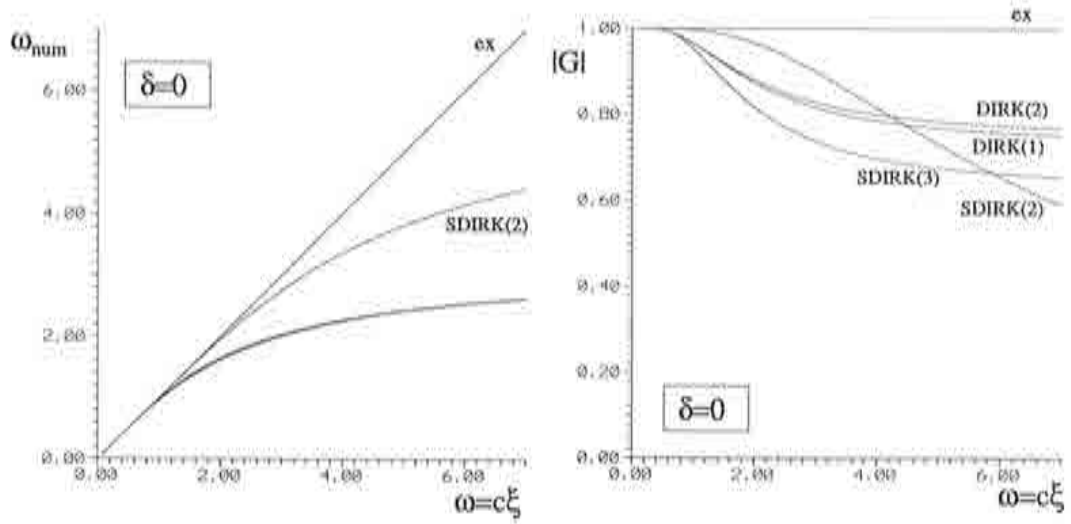

Figure 9: Accuracy of DIRK methods for pure convection.

From the preceding results we can conclude that if $R(z) = P(z)/Q(z)$ is an irreducible A-stable polinomial quotient satisfying $R(z) - e^z = O(z^{n+1})$. Then there exists an s-stage n-order exponential method with $R(z)$ as stability function ($s \leq \deg(Q) + \deg(P)$). And also there exists an s-stage n-order Runge-Kutta method with $R(z)$ as stability function ($s = \deg(Q)$). Both methods are equivalent. The difference in linear problems is only the implementation. Note that it is easy to find the exponential method and it is quite dificult to find the equivalent Runge-Kutta method.

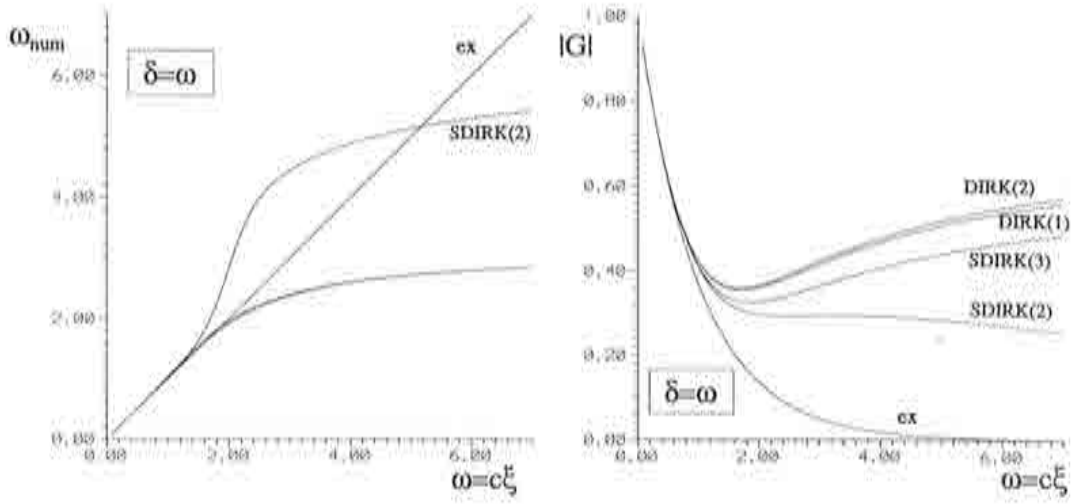

Figure 10: Accuracy of DIRK methods for convection-diffusion.

What is important is not only the numerical schemes but the accuracy. The phase and damping precision of DIRK methods are shown in Figures 9-11. It is possible to see that always the Padé schemes (Fig. 5-7) have better accuracy than DIRK methods. Other autors have also noticed that the DIRK's methods are generally disappointing [10, 23, 27].

All the implicit methods considered are A-stable, so they haven't any stability restriction. The limit on Δt comes from accuracy considerations. Let h the spatial increment, $\xi = kh$ the dimensionless wave number, k the dimensional wave number and c and d the Courant number and the diffusive factor respectively. The region of accurate spatial resolution is $0 \leq \xi \leq \frac{\pi}{4}$. That means $0 \leq k \leq \frac{\pi}{4h}$. The exact damping and frequency are $\delta = d\xi^2$ and $\omega = c\xi$. Then the important

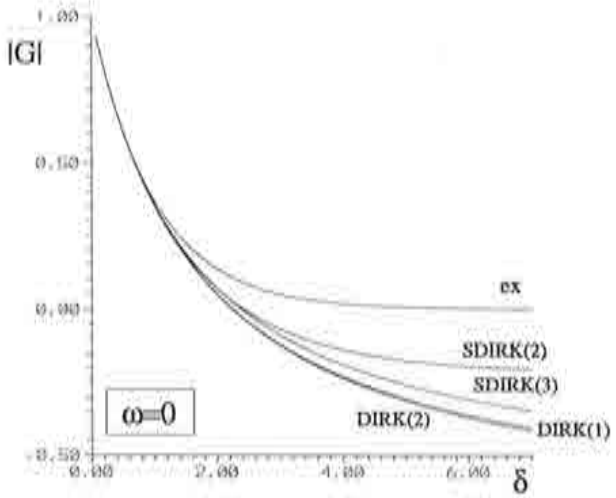

Figure 11: Accuracy of DIRK methods for pure diffusion.

regions are $0 \leq \omega \leq c\frac{\pi}{4}$ and $0 \leq \delta \leq d\frac{\pi^2}{16}$. If ω_p and δ_p are the limits on precision we obtain the following accuracy limits on the Courant number and the difussive factor

$$\begin{array}{rcl} c & \leq & \omega_p \frac{4}{\pi} \simeq 1.27324\,\omega_p \\ d & \leq & \frac{16}{\pi^2}\delta_p \simeq 1.62114\,\delta_p \end{array} \tag{117}$$

Let ϵ the tolerance of error that we admit, that is, $|e^z - R(z)| < \epsilon$. ω_p and δ_p are the maximum satisfying $|e^z - R(z)| < \epsilon$ where $z = \delta + i\omega$, i.e. ,

$$\begin{array}{rcl} \omega_p & = & \max\left\{\omega\,;\,\left|e^{\delta+i\omega} - R(\delta+i\omega)\right| \leq \epsilon,\ \delta \in I_\delta\right\} \\ \delta_p & = & \max\left\{\delta\,;\,\left|e^{\delta+i\omega} - R(\delta+i\omega)\right| \leq \epsilon,\ \omega \in I_\omega\right\} \end{array} \tag{118}$$

where I_δ is the interval of damping and I_ω the interval of frequencies on consideration. It is also possible to consider a different tolerance for phase and damping errors.
Notice that the accuracy limits on DIRK methods are too restrictive for a given ϵ, $(0 < \epsilon \ll 1)$. The Padé methods have higher accuracy limits. It seems that the more accurate A-stable family of methods are the A-stable multistage Padé schemes, or equivalently, the classical implicit Runge-Kutta methods.

7 Implicit schemes based on Simpson's quadrature rule

Consider the partial differential equation

$$\frac{\partial u}{\partial t} = R(u) \tag{119}$$

where R represents the advection-diffusion operator. Over a typical time step $\Delta t = t^{n+1} - t^n$, the change of u is given by

$$u^{n+1} - u^n = \int_{t^n}^{t^{n+1}} \frac{\partial u}{\partial t}\,dt. \tag{120}$$

We shall exploit this relationship to rediscover some classical implicit time stepping schemes with high-order accuracy in the time step.
To evaluate the integral in the right-hand side of the above equation, we shall use polynomial approximations for $\frac{\partial u}{\partial t}$ which, as before, will be denoted u_t. Using the normalised coordinate ξ $(-1 \leq \xi \leq 1)$, we write

$$t = \frac{1}{2}(1-\xi)\,t^n + \frac{1}{2}(1+\xi)\,t^{n+1} \tag{121}$$

$$dt = \frac{t^{n+1} - t^n}{2}d\xi = \frac{\Delta t}{2}d\xi \tag{122}$$

so that expression (120) reads

$$u^{n+1} - u^n = \frac{\Delta t}{2} \int_{-1}^{+1} u_t(\xi)\, d\xi. \tag{123}$$

We shall now successively consider linear, quadratic and cubic polynomial approximations to $u_t(\xi)$.

7.1 Linear approximation

If u_t is assumed to vary linearly from t^n to t^{n+1}, i.e.

$$u_t(\xi) = \frac{1}{2}(1-\xi)\, u_t^n + \frac{1}{2}(1+\xi)\, u_t^{n+1} \tag{124}$$

one obtains from (120) the well-known trapezoidal rule, or Crank-Nicolson scheme

$$u^{n+1} - u^n = \frac{\Delta t}{2}\left(u_t^n + u_t^{n+1}\right), \tag{125}$$

which is second-order accurate in the time step Δt.

7.2 Quadratic approximation

Let us now assume that u_t has a quadratic variation over the time interval Δt given in terms of the normalised coordinate ξ by

$$u_t(\xi) = \frac{1}{2}\xi(\xi-1)\, u_t^n + (1-\xi^2)\, u_t^{n+\frac{1}{2}} + \frac{1}{2}\xi(\xi+1)\, u_t^{n+1} \tag{126}$$

Introducing this expression into (123) we find the scheme

$$u^{n+1} - u^n = \frac{\Delta t}{6}\left(u_t^n + 4u_t^{n+\frac{1}{2}} + u_t^{n+1}\right) \tag{127}$$

This is a fourth-order accurate generalization of Simpson's quadrature as can be verified by inserting the following Taylor series in the above scheme:

$$u_t^{n+\frac{1}{2}} = u_t^n + \frac{\Delta t}{2}u_{tt}^n + \frac{\Delta t^2}{8}u_{ttt}^n + \frac{\Delta t^3}{48}u_{tttt}^n + O(\Delta t^4) \tag{128}$$

$$u_t^{n+1} = u_t^n + \Delta t\, u_{tt}^n + \frac{\Delta t^2}{2}u_{ttt}^n + \frac{\Delta t^3}{6}u_{tttt}^n + O(\Delta t^4) \tag{129}$$

Scheme (127) involves three time levels and can therefore not be directly implemented. A two-stage implementation of the scheme is required which reads

$$u^{n+\frac{1}{2}} - u^n = \frac{\Delta t}{24}\left(5u_t^n + 8u_t^{n+\frac{1}{2}} - u_t^{n+1}\right) \tag{130}$$

$$u^{n+1} - u^{n+\frac{1}{2}} = \frac{\Delta t}{24}\left(-u_t^n + 8u_t^{n+\frac{1}{2}} + 5u_t^{n+1}\right) \tag{131}$$

The expression for $u^{n+\frac{1}{2}}$ results from the integration of relation (126) from t^n to $t^{n+\frac{1}{2}}$, while the expression for u^{n+1} arises from the integration from $t^{n+\frac{1}{2}}$ to t^{n+1}. In the case of pure convection, second time derivatives can be incorporated in the time integration scheme and one might consider eliminating the intermediate value $u_t^{n+\frac{1}{2}}$ using the forward and backward approximations

$$u_t^{n+\frac{1}{2}} = u_t^n + \frac{\Delta t}{2} u_{tt}^n + \frac{\Delta t^2}{8} u_{ttt}^n + O(\Delta t^3) \tag{132}$$

$$u_t^{n+\frac{1}{2}} = u_t^{n+1} - \frac{\Delta t}{2} u_{tt}^{n+1} + \frac{\Delta t^2}{8} u_{ttt}^{n+1} + O(\Delta t^3) \tag{133}$$

Taking the arithmetic mean of the above expressions gives

$$u_t^{n+\frac{1}{2}} = \frac{1}{2}\left(u_t^n + u_t^{n+1}\right) + \frac{\Delta t}{4}\left(u_{tt}^n - u_{tt}^{n+1}\right) + \frac{\Delta t^2}{16}\left(u_{ttt}^n + u_{ttt}^{n+1}\right) \tag{134}$$

and noting that

$$u_{tt}^{n+1} - u_{tt}^n = \frac{\Delta t}{2}\left(u_{ttt}^n + u_{ttt}^{n+1}\right) + O(\Delta t^2) \tag{135}$$

one obtains

$$u_t^{n+\frac{1}{2}} = \frac{1}{2}\left(u_t^n + u_t^{n+1}\right) + \frac{\Delta t}{8}\left(u_{tt}^n - u_{tt}^{n+1}\right) \tag{136}$$

Now, introducing this expression into relation (127) yields

$$u^{n+1} - u^n = \frac{\Delta t}{2}\left(u_t^n + u_t^{n+1}\right) + \frac{\Delta t^2}{12}\left(u_{tt}^n - u_{tt}^{n+1}\right) \tag{137}$$

This is the fourth-order accurate time stepping scheme of Harten and Tal-Ezer corresponding to Padé approximation $R_{2,2}$ in Table 8.

7.3 Cubic approximation

Let us now assume that the time derivative u_t has a cubic variation over the time interval Δt.

To define u_t, we shall use a cubic expansion based upon four nodes located at the Lobatto points

$$\xi = -1.0, -\frac{1}{\sqrt{5}}, +\frac{1}{\sqrt{5}}, +1.0$$

and upon Lagrange shape functions defined in terms of the normalized coordinate ξ by

$$N_1(\xi) = \frac{5}{8}(1-\xi)(\xi^2 - \frac{1}{5})$$

$$N_2(\xi) = \frac{5\sqrt{5}}{8}(\xi - \frac{\sqrt{5}}{5})(\xi^2 - 1)$$

$$
\begin{aligned}
N_3(\xi) &= -\frac{5\sqrt{5}}{8}\left(\xi + \frac{\sqrt{5}}{5}\right)\left(\xi^2 - 1\right) \\
N_4(\xi) &= \frac{5}{8}\left(1 + \xi\right)\left(\xi^2 - \frac{1}{5}\right)
\end{aligned}
\tag{138}
$$

The cubic variation of u_i is then expressed in the form:

$$
u_i(\xi) = \sum_{l=1}^{4} N_l(\xi)\, u_{il}, \tag{139}
$$

where

$$
\begin{aligned}
u_{i1} &= u_i^n \\
u_{i2} &= u_i^{n+\alpha} \\
u_{i3} &= u_i^{n+\beta} \\
u_{i4} &= u_i^{n+1}
\end{aligned}
\tag{140}
$$

where we have posed

$$
\alpha = \frac{5 - \sqrt{5}}{10} \qquad \beta = \frac{5 + \sqrt{5}}{10}
$$

Now, introducing expression (139) into relationship (123), we obtain the scheme

$$
u^{n+1} - u^n = \frac{\Delta t}{12}\left(u_i^n + 5\,u_i^{n+\alpha} + 5\,u_i^{n+\beta} + u_i^{n+1}\right). \tag{141}
$$

This is a sixth-order accurate generalization of Simpson's quadrature, as can be verified by development into Taylor series around time t^n. Its stability function is $R_{3,3}(z)$ (see Section 6.4). Scheme (141) involves four time levels and, like the quadratic scheme, it must be implemented into stages. Three stages are needed in the present case and they correspond to the intermediate time levels $t^{n+\alpha}$, $t^{n+\beta}$, and to the end-of-step time level t^{n+1}.

To obtain the equations governing the three stages, we first integrate expression (139) for $u_i(\xi)$ from time t^n to time $t^{n+\alpha}$, then from $t^{n+\alpha}$ to $t^{n+\beta}$, and finally from $t^{n+\beta}$ to time t^{n+1}.

This gives the following equations for the three stages of the sixth-order scheme:

$$
\begin{aligned}
u^{n+\alpha} - u^n &= \frac{\Delta t}{120}\Big((11 + \sqrt{5})u_i^n + (25 - \sqrt{5})u_i^{n+\alpha} + (25 - 13\sqrt{5})u_i^{n+\beta} \\
&\quad -(1 - \sqrt{5})u_i^{n+1}\Big) \\
u^{n+\beta} - u^{n+\alpha} &= \frac{\Delta t}{120}\left(-2\sqrt{5}u_i^n + 14\sqrt{5}u_i^{n+\alpha} + 14\sqrt{5}u_i^{n+\beta} - 2\sqrt{5}u_i^{n+1}\right) \\
u^{n+1} - u^{n+\beta} &= \frac{\Delta t}{120}\Big(-(1 - \sqrt{5})u_i^n + (25 - 13\sqrt{5})u_i^{n+\alpha} + (25 - \sqrt{5})u_i^{n+\beta} \\
&\quad +(11 + \sqrt{5})u_i^{n+1}\Big)
\end{aligned}
\tag{142}
$$

Since the sixth-order scheme involves three coupled equations, it will be very expensive to use. Therefore, a critical assessment of the advantage of a higher accuracy against the increased computational cost should be made before using such a scheme in practical applications.

8 Numerical results

Numerical tests were performed to assess the performance of selected implicit Padé schemes of high order in the solution of convection and convection-diffusion problems.
The selected schemes are $R_{1,2}$, $R_{2,2}$, $R_{2,3}$ and $R_{3,3}$.

8.1 Convection-Diffusion of a Gaussian Profile

To illustrate the performance of the selected high-order Padé schemes and compare them to standard explicit schemes, consider first the linear convection-diffusion problem over the spatial interval $[0, 150]$ defined by the following initial and boundary conditions:

$$\begin{aligned} u(x,0) &= \frac{2.5}{\sigma} e^{-\frac{1}{2}X^2} \\ u(0,t) &= 0 \\ u(150,t) &= \frac{2.5}{\sigma_1} e^{-\frac{1}{2}L^2} \end{aligned} \tag{143}$$

with $X = (x - x_0)/\sigma$, $\sigma = 3.5$, $L = (150 - x_0 - t)/\sigma_1$, $\sigma_1 = \sigma\sqrt{1 + 2\nu t/\sigma^2}$ and $x_0 = 20$ for $Pe = 5$ and $x_0 = 60$ for $Pe = 0.1$. A unit convection velocity is assumed and the calculations were made using a uniform mesh of linear elements with $h = 1$.
In Figs. 12 to 17, we compare the profiles of the Gaussian obtained at various time levels with the implicit Padé schemes $R_{1,2}$, $R_{2,2}$, $R_{2,3}$ and $R_{3,3}$ with the three-stage explicit scheme $R_{3,0}$ (3TG) and with the second order explicit scheme of Peraire [19] (TG2Pe). Two values of the Péclet number were considered,

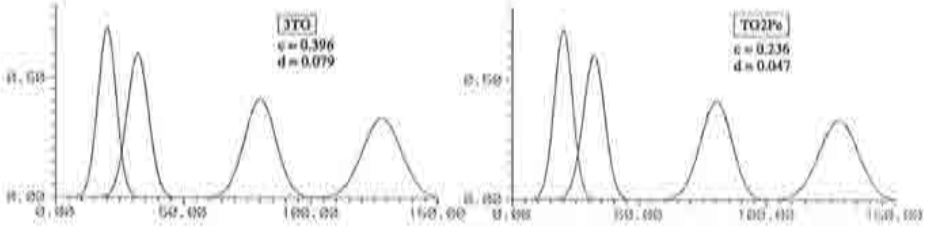

Figure 12: Convection-diffusion of a Gaussian by 3TG [15] and TG2Pe [19] with $Pe = 5$ for $t = 0$, 12, 60, 108.

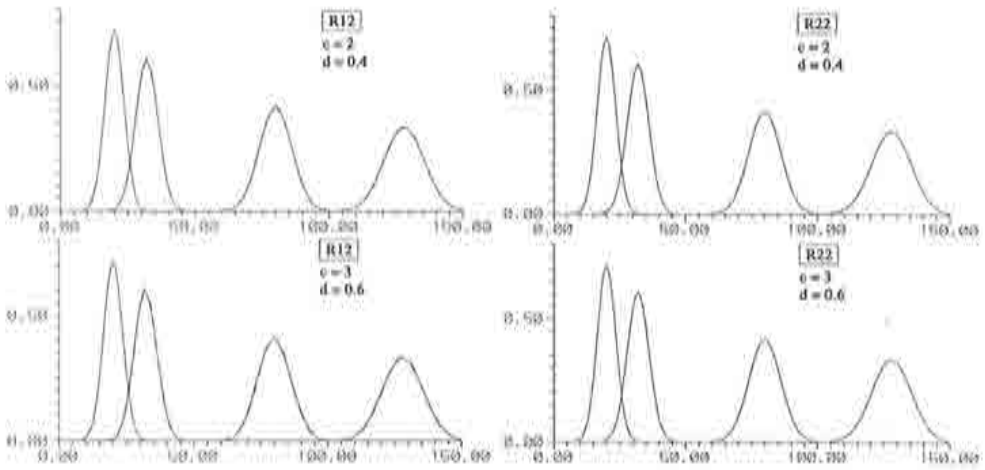

Figure 13: Convection-diffusion of a Gaussian by $R_{1,2}$ and $R_{2,2}$ with $Pe = 5$ at $c = 2,\ 3$ for $t = 0,\ 12,\ 60,\ 108$.

namely $Pe = 0.1$ and $Pe = 5$. The results for $Pe = 0.1$ are at times $t = 0,\ 2,\ 6,\ 24$, while they are at times $t = 0,\ 12,\ 60,\ 108$ for $Pe = 5$. The explicit schemes were operated with a time step equal to 90 percent of their critical value, while the implicit ones used large values of the Courant number c to appraise their accuracy well beyond the stability limit of the explicit schemes. The results indicate that the implicit schemes can produce very accurate answers for large values of the time step. The discontinuous lines in Figs. 12 to 17 correspond to the analytical solution of the problem.

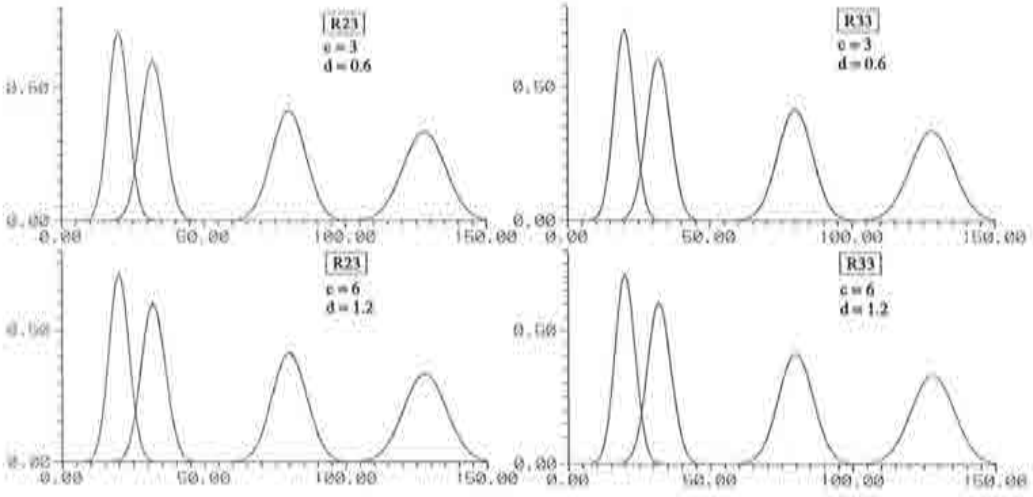

Figure 14: Convection-diffusion of a Gaussian by $R_{2,3}$ and $R_{3,3}$ with $Pe = 5$ at $c = 3,\ 6$ for $t = 0,\ 12,\ 60,\ 108$.

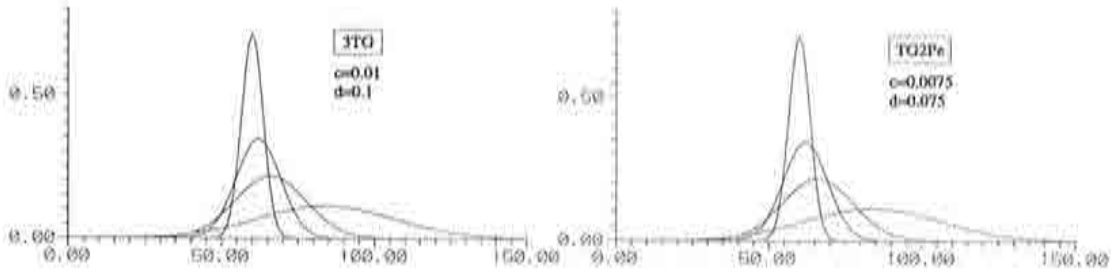

Figure 15: Convection-diffusion of a Gaussian by 3TG [15] and TG2Pe [19] with $Pe = 0.1$ for $t = 0,\ 2,\ 6,\ 24$.

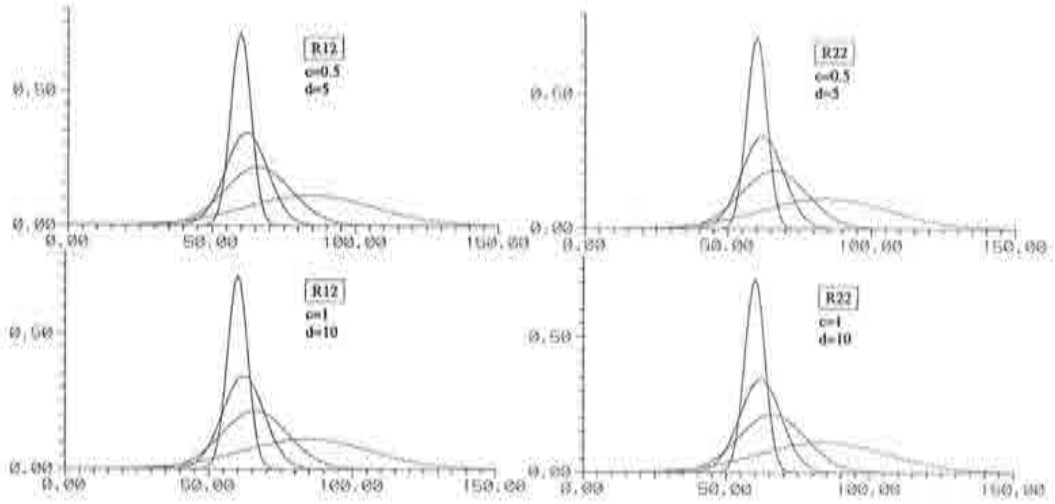

Figure 16: Convection-diffusion of a Gaussian by $R_{1,2}$ and $R_{2,2}$ with $Pe = 0.1$ at $c = 0.5,\ 1$ for $t = 0,\ 2,\ 6,\ 24$.

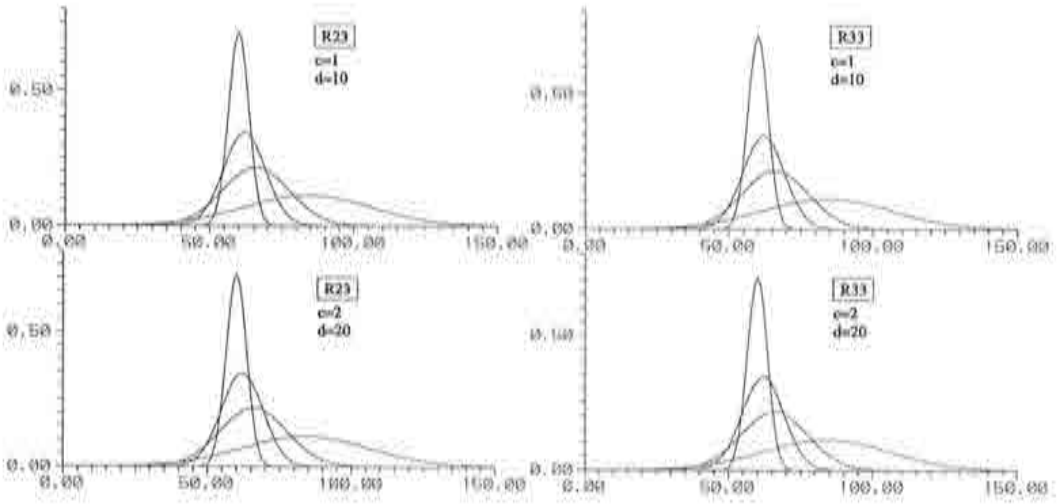

Figure 17: Convection-diffusion of a Gaussian by $R_{2,3}$ and $R_{3,3}$ with $Pe = 0.1$ at $c = 1,\ 2$ for $t = 0,\ 2,\ 6,\ 24$.

8.2 Rotating Cosine Hill

This standard test problem considers the convection of a product cosine hill in a 2D pure rotation velocity field. The initial conditions are

$$u(\boldsymbol{x},0) = \begin{cases} \frac{1}{4}\left[1+\cos\pi X_1\right]\left[1+\cos\pi X_2\right] & \text{if } X_1^2+X_2^2 \le 1 \\ 0 & \text{otherwise} \end{cases}$$

where $\boldsymbol{X} = (\boldsymbol{x}-\boldsymbol{x}_0)/\sigma$, $\boldsymbol{x}_0$ and σ being the initial position of the centre and the radius of the cosine hill. The advection field is a pure rotation with unit angular velocity given by $\boldsymbol{a}(\boldsymbol{x}) = (-x_2, x_1)$

A uniform mesh of 30×30 quadrilateral elements over the unit square $[-\frac{1}{2},\frac{1}{2}] \times [-\frac{1}{2},\frac{1}{2}]$ has been employed in the calculations of the Figures 18-19 and the standard Galerkin finite element method has been used for the spatial discretization. Here again, the implicit methods $R_{1,2}$, $R_{2,2}$, $R_{2,3}$ and $R_{3,3}$ are compared to the explicit schemes $3TG$ and $TG2Pe$. The numerical solutions for the case $\boldsymbol{x}_0 = (\frac{1}{6},\frac{1}{6})$ and $\sigma = 0.2$ are shown in Figs. 18 and 19. They give the elevations of the rotating cosine hill after one full revolution. To compare the accuracy of the various schemes, the maximum and minimum values of the numerical solutions are provided, together with the value of the maximum Courant number in the finite element mesh computed in the middle of the sides of the boundary. One notes that by contrast with the explicit schemes the implicit methods can be accurately operated with quite large time steps. Scheme $R_{1,2}$ appears to be the less accurate implicit A-stable method as could be expected from the accuracy properties shown in Figs. 5-7.

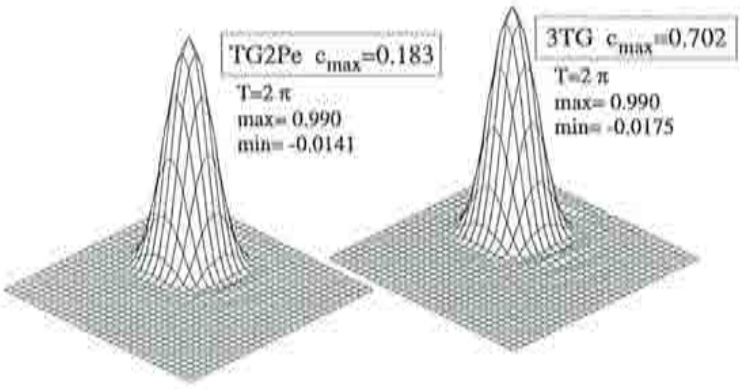

Figure 18: Solution of the Rotating Cosine Hill using $3TG$ and $TG2Pe$ explicit methods.

Table 30 shows a relation between precision and cost in a non structured mesh (Fig. 20) with 4501 bilinear elements and 4576 nodes. The spatial increment is $h_{\min} = 0.004$, $h_{\max} = 0.08$, $h_{\text{mean}} = 0.012415$. We have done only one descomposition of the matrix. It is possible to see that the new implicit schemes are more efficient than the explicit ones maintaining good accuracy.

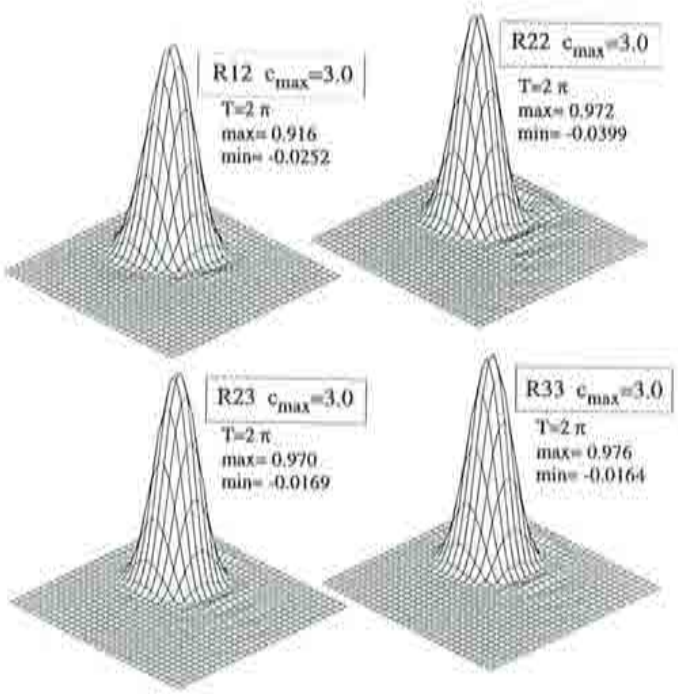

Figure 19: Solution of the Rotating Cosine Hill with the implicit Padé schemes $R_{1,2}$, $R_{2,2}$, $R_{2,3}$ and $R_{3,3}$ for $c = 3$.

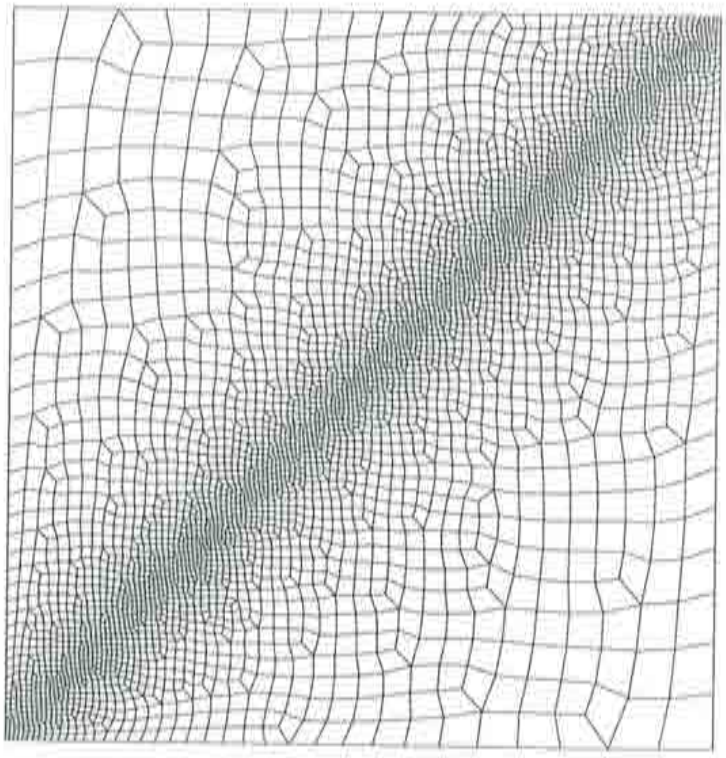

Figure 20: Non structured mesh used with the rotating cosine hill.

method	time	time steps	c_{max}	CPU	u_{max}	u_{min}
R12	2π	264	3	282	1.01150	-0.04991
R22	2π	264	3	286	1.01418	-0.04973
R23	2π	264	3	653	1.01150	-0.05074
R33	2π	264	3	637	1.01019	-0.05116
TG2pe	2π	4276	0.1837	1657	0.99144	-0.03012
TG3	2π	1120	0.702	1297	1.00592	-0.05194
R12	20π	2620	3	2338	1.10229	-0.21855
R22	20π	2620	3	2475	1.10889	-0.21304
R23	20π	2620	3	4685	1.10270	-0.22145
R33	20π	2620	3	4387	1.10001	-0.22505
TG2pe	20π	42752	0.1837	16879	1.04292	-0.08770
TG3	20π	11189	0.702	12723	1.08634	-0.24244

Table 30: Results for the rotating cosine hill without diffusion with the non structured mesh (CPU in seconds).

8.3 Rotating Cosine Hill with Diffusion

This is an advection-diffusion problem and its description is the same as in the previous example, except that physical diffusion has been added to give a maximum value of the Péclet number of 20.
As before, the Padé implicit schemes are compared to second- and third-order accurate explicit methods.
The numerical solutions obtained after a complete revolution are shown in Figs. 21 to 25. No analytical solution is available in the present case and the various schemes have to be compared between them. The Padé schemes can work with high Courant numbers without losing significant accuracy.

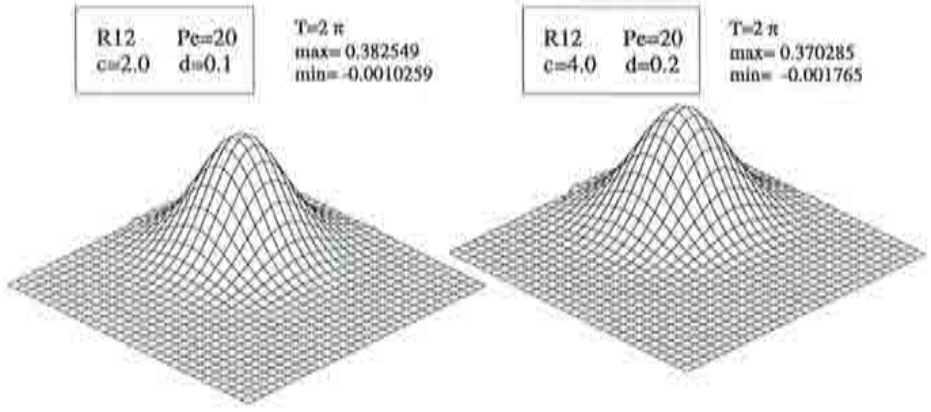

Figure 21: Solution of the Rotating Cosine Hill with diffusion by $R_{1,2}$.

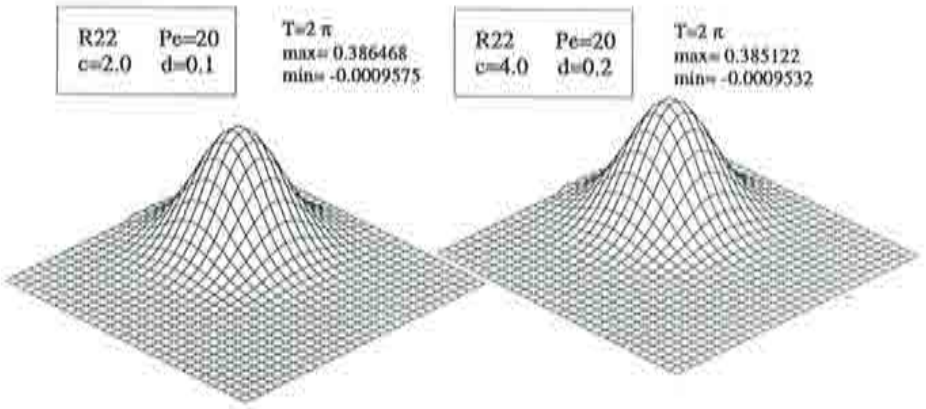

Figure 22: Solution of the Rotating Cosine Hill with diffusion by $R_{2,2}$.

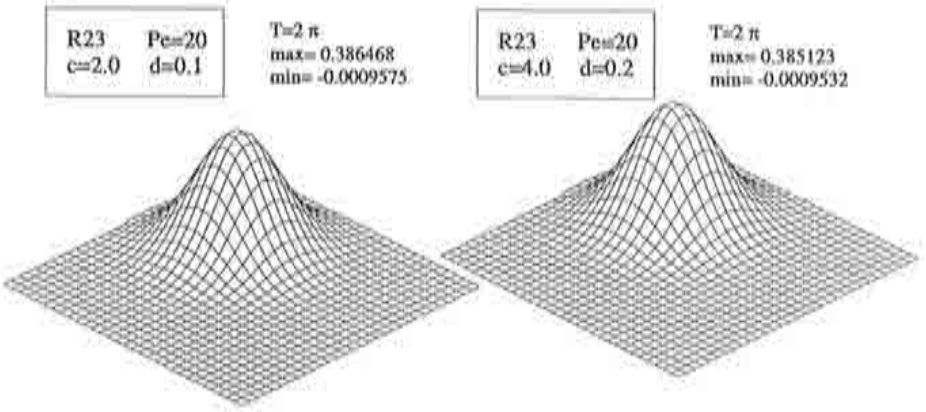

Figure 23: Solution of the Rotating Cosine Hill with diffusion by $R_{2,3}$.

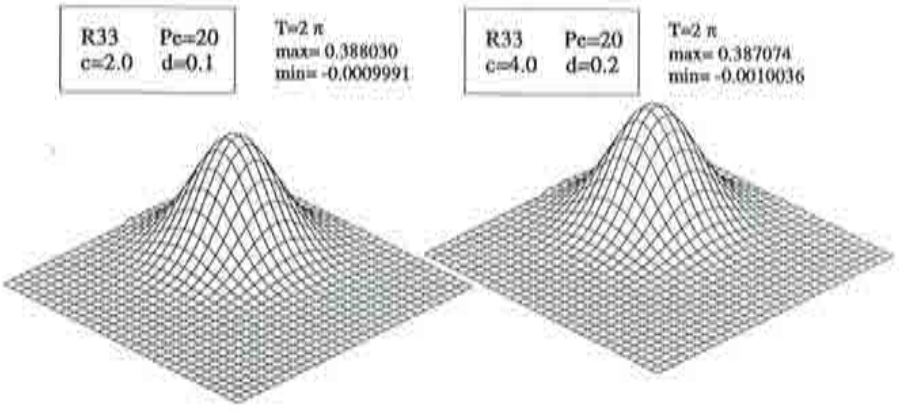

Figure 24: Solution of the Rotating Cosine Hill with diffusion by $R_{3,3}$.

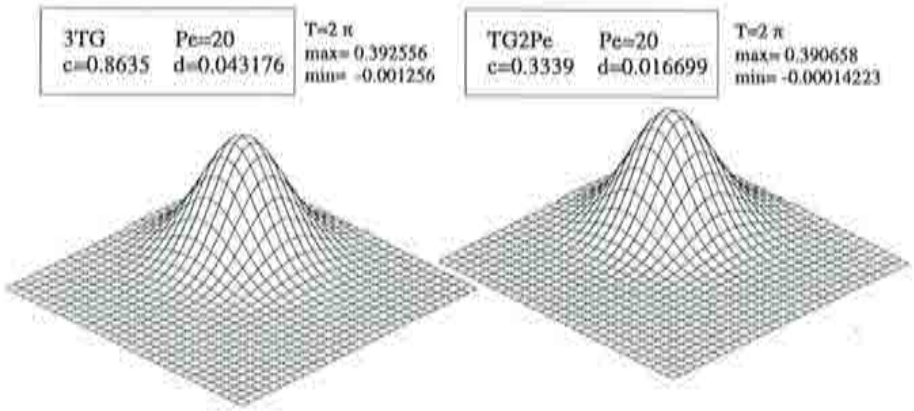

Figure 25: Solution of the Rotating Cosine Hill with diffusion by 3TG and TG2Pe.

8.4 Burgers equation in 1D

One of the main objectives of the A-stable implicit methods is to solve nonlinear stiff problems. As a first nonlinear test, we have solved the Burgers advection-diffusion equation in 1D to appraise the performance of the high-order Padé schemes with respect to the standard explicit schemes. We consider the Burgers problem over the spatial interval $[0, 1]$ defined by

$$\begin{aligned} u_t + uu_x &= \nu u_{xx} \\ u(x,0) &= \sin(\pi x) \\ u(0,t) &= u(1,t) = 0 \end{aligned} \tag{144}$$

for $Pe = 1$ and $\nu = 0.001$. A uniform mesh of linear elements of size $h = 0.001$ has been used.

Figures 28 to 26 show the results obtained with both implicit and explicit methods and one can appreciate the efficiency of the high order Padé methods from the test data in Table 31. The $R_{2,3}$ and the $R_{3,3}$ methods are more than seven times faster than the TG2Pe method, and more than seventeen times faster than the 3TG method. The explicit schemes were operated with a time step equal to 75 percent of their critical value, while $R_{2,3}$ and $R_{3,3}$ used large values of the Courant number c. Note that in the $R_{2,3}$ and $R_{3,3}$ methods a nonlinear system had to be solved at each time station by Newton-Raphson iteration. Only two iterations were needed to obtain an accuracy in excess of 10^{-4}.

This simple test problem provides a good illustration of the penalization introduced by the conditional stability of explicit methods when a refined spatial discretization of convection–diffusion problems is required.

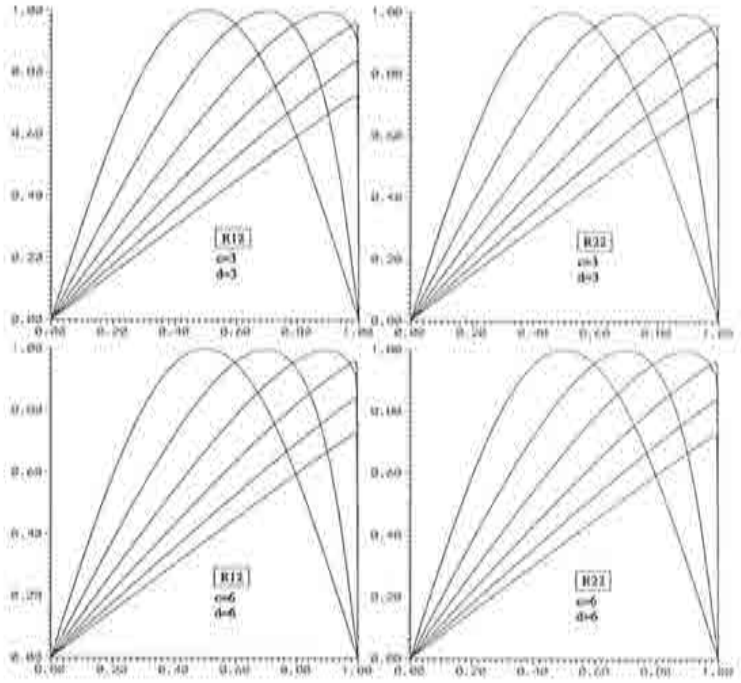

Figure 26: Solution of 1D Burgers equation by $R_{1,2}$ and $R_{2,2}$ with $Pe = 1$ at $c = 3, 6$ for $t = 0, 0.2, 0.4, 0.6, 0.8, 1.0$.

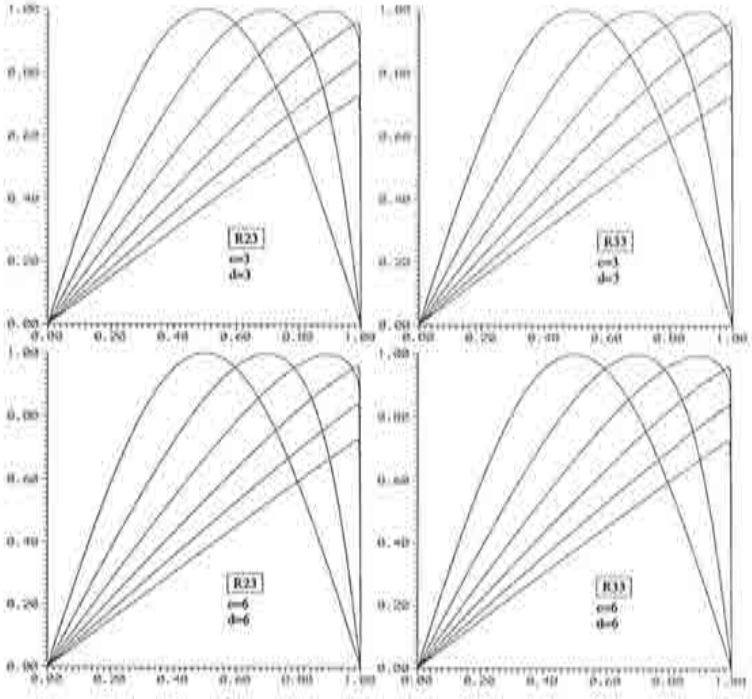

Figure 27: Solution of 1D Burgers equation by $R_{2,3}$ and $R_{3,3}$ with $Pe = 1$ at $c = 3, 6$ for $t = 0, 0.2, 0.4, 0.6, 0.8, 1.0$.

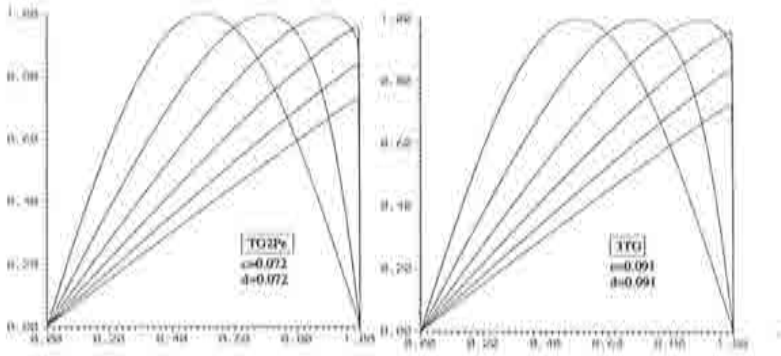

Figure 28: Solution of 1D Burgers equation by 3TG [15] and TG2Pe [19] with $Pe = 1$ for $t = 0, 0.2, 0.4, 0.6, 0.8, 1.0$.

method	c_{max}	d	Δt	CPU	Time steps
TG2Pe	0.072	0.072	0.000072	2215	13809
3TG	0.0907	0.0907	0.0000907	5216	10998
R12	3	3	0.003	237	335
R12	6	6	0.006	126	170
R22	3	3	0.003	263	335
R22	6	6	0.006	141	170
R23	3	3	0.003	537	335
R23	6	6	0.006	280	170
R33	3	3	0.003	572	335
R33	6	6	0.006	306	170

Table 31: Comparison of implicit Padé schemes and explicit methods for the 1D Burgers problem.

8.5 Nonlinear convection-diffusion problem in 2D

As a last test case, we consider the solution of a new 2D Burgers problem over the square domain $\Omega = [0, 1] \times [0, 1]$ for which an analytical solution can be devised, thus allowing a direct assessment of the quality of the numerical results obtained with the high-order Padé schemes.
The problem is defined by the equations

$$\begin{aligned} u_t + (u, v) \cdot \nabla u &= \nu \nabla^2 u \\ v_t + (u, v) \cdot \nabla v &= \nu \nabla^2 v, \end{aligned} \tag{145}$$

which are coupled through their nonlinear convective terms, and by the following

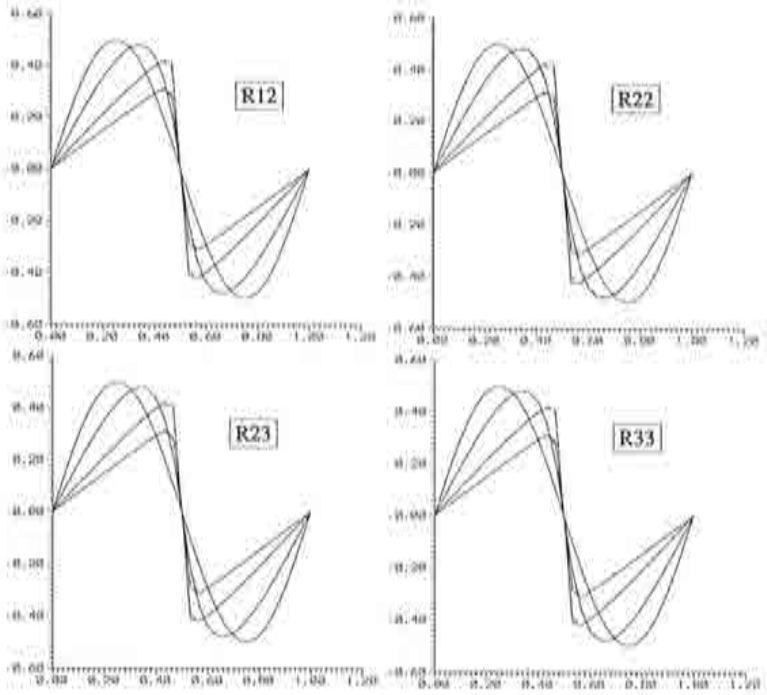

Figure 29: Solution $u(x,x,t)$ of 2D Burgers problem by $R_{1,2}$, $R_{2,2}$, $R_{2,3}$ and $R_{3,3}$ with $Pe = 3.33$, $c = 3$, $d = 0.9$ for $t = 0,\ 0.2,\ 0.6,\ 1$.

initial and boundary conditions:

$$\begin{aligned} &u(x,y,0) = \sin(\pi x)\cos(\pi y) \qquad v(x,y,0) = \cos(\pi x)\sin(\pi y) \\ &u(0,y,t) = u(1,y,t) = 0 \qquad v(x,0,t) = v(x,1,t) = 0 \\ &\frac{\partial u}{\partial n}(x,0,t) = \frac{\partial u}{\partial n}(x,1,t) = 0 \quad \frac{\partial v}{\partial n}(0,y,t) = \frac{\partial v}{\partial n}(1,y,t) = 0 \end{aligned} \tag{146}$$

The analytical solution to the above Burgers problem is given by

$$\begin{aligned} u(x,y,t) &= -2\nu\frac{\Phi_x(x,y,t)}{\Phi(x,y,t)} \\ v(x,y,t) &= -2\nu\frac{\Phi_y(x,y,t)}{\Phi(x,y,t)} \end{aligned} \tag{147}$$

where

$$\begin{aligned} \Phi(x,y,t) &= \sum_{n,m=0}^{\infty} a_{nm}\cos(n\pi x)\cos(m\pi y)e^{-(n^2+m^2)\nu\pi^2 t} \\ \Phi_x(x,y,t) &= -\pi\sum_{n=1,m=0}^{\infty} a_{nm}n\sin(n\pi x)\cos(m\pi y)e^{-(n^2+m^2)\nu\pi^2 t} \\ \Phi_y(x,y,t) &= -\pi\sum_{n=0,m=1}^{\infty} a_{nm}m\cos(n\pi x)\sin(m\pi y)e^{-(n^2+m^2)\nu\pi^2 t} \end{aligned} \tag{148}$$

and a_{nm} are the coefficients of a double Fourier series defined by

$$\begin{aligned} a_{00} &= \int_0^1 \int_0^1 e^{\cos(\pi x)\cos(\pi y)/(2\nu\pi)}\, dx\, dy \\ a_{n0} = a_{0n} &= 2\int_0^1 \int_0^1 e^{\cos(\pi x)\cos(\pi y)/(2\nu\pi)} \cos(n\pi x)\, dx\, dy \\ a_{nn} = a_{mn} &= 4\int_0^1 \int_0^1 e^{\cos(\pi x)\cos(\pi y)/(2\nu\pi)} \cos(n\pi x)\cos(m\pi y)\, dx\, dy. \end{aligned} \tag{149}$$

The problem defined by Eqs.(145) and (146) exhibits various symmetries. For instance, along a transverse section of the domain one has $u(x,x,t) = v(x,x,t)$ and $u(x,x,t) = -u(1-x,1-x,t)$. Moreover, one has $u(x,y,t) = v(y,x,t)$ and $u(x,y,t) = -u(1-x,1-y,t)$ over the global domain.
When convection dominates the nonlinear transport, the solution includes the formation of a shock along the diagonal of the domain passing through the points $(0,1)$ and $(1,0)$. Since a conventional Galerkin method is used herein for the spatial representation, the numerical solutions were computed for a moderate value of the Péclet number in order to avoid unphysical oscillations. The results obtained on a uniform mesh of 30×30 bilinear elements with both explicit and implicit methods are shown in Figs. 29 to 36. The results along the domain diagonal reported in Figs. 29 and 30 are compared to the exact solution which is represented by discontinuous lines. Because a rather coarse mesh has been employed in the present test problem, the explicit methods could be operated with rather large time steps (80% of the critical value) and were found to be competitive with respect to the implicit methods as regards the computing time needed to complete the problem.

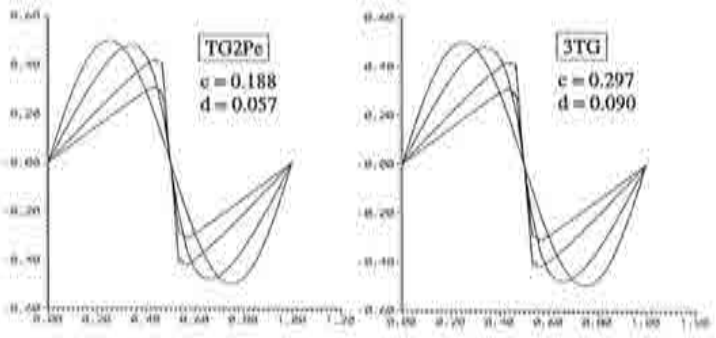

Figure 30: Solution $u(x,x,t)$ of 2D Burgers problem by $TG2Pe$ and $3TG$ with $Pe = 3.33$ for $t = 0,\ 0.2,\ 0.6,\ 1.$

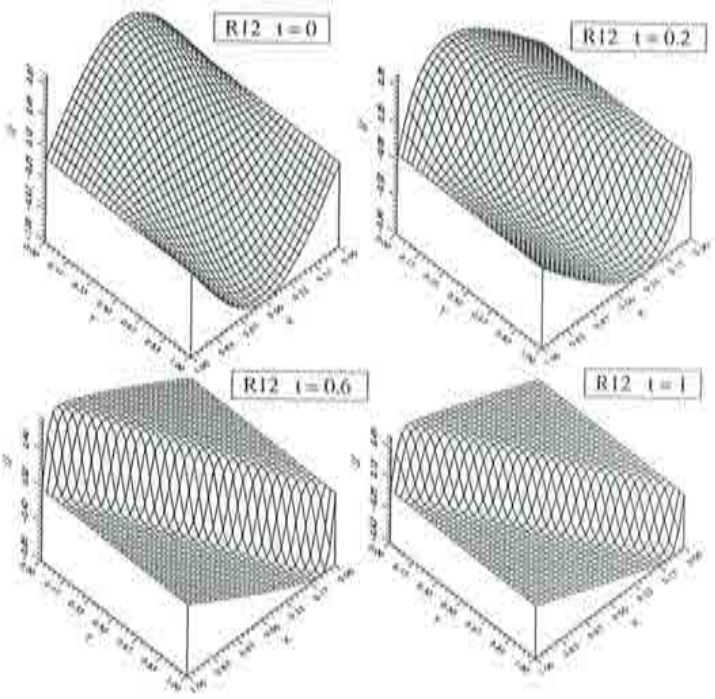

Figure 31: Solution $u(x, y, t)$ of 2D Burgers problem by $R_{1,2}$ with $Pe = 3.33$ for $c = 3$, $d = 0.9$.

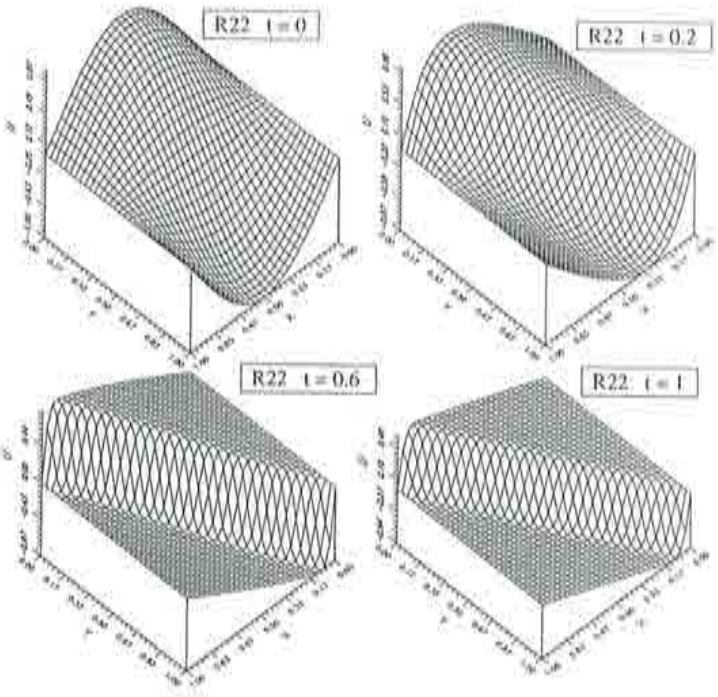

Figure 32: Solution $u(x, y, t)$ of 2D Burgers problem by $R_{2,2}$ with $Pe = 3.33$ for $c = 3$, $d = 0.9$.

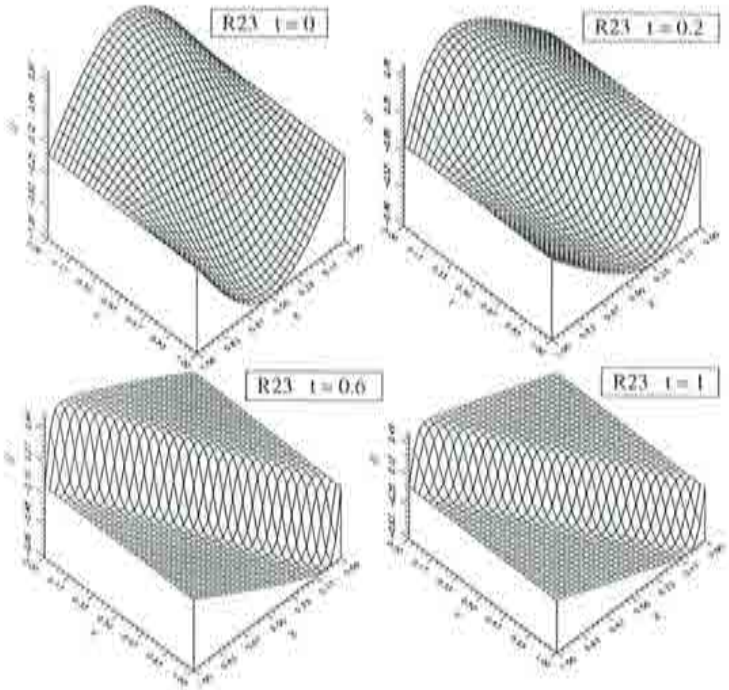

Figure 33: Solution $u(x, y, t)$ of 2D Burgers problem by $R_{2,3}$ with $Pe = 3.33$ for $c = 3$, $d = 0.9$.

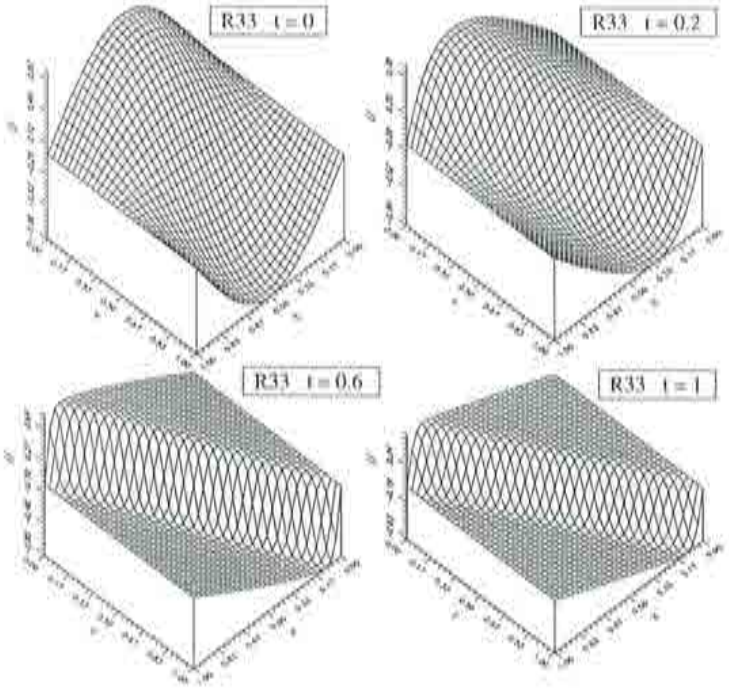

Figure 34: Solution $u(x, y, t)$ of 2D Burgers problem by $R_{3,3}$ with $Pe = 3.33$ for $c = 3$, $d = 0.9$.

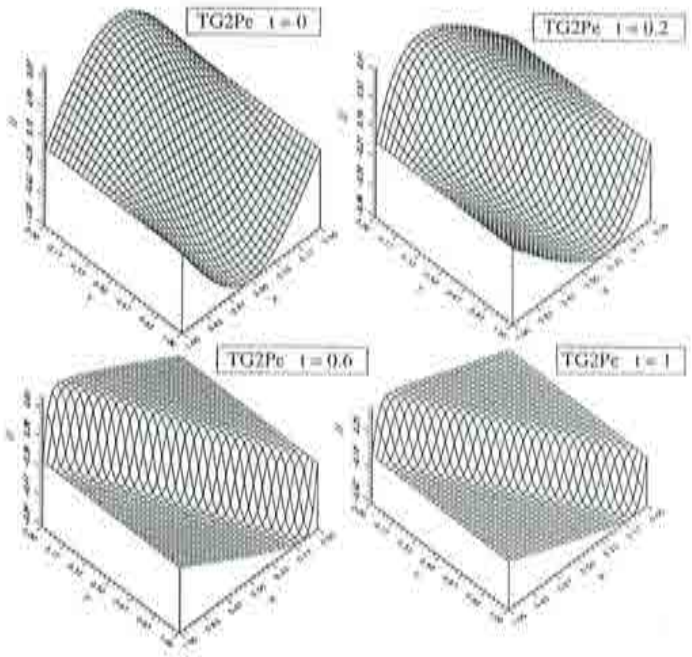

Figure 35: Solution $u(x, y, t)$ of 2D Burgers problem by $TG2Pe$ with $Pe = 3.33$ for $c = 0.18$, $d = 0.057$.

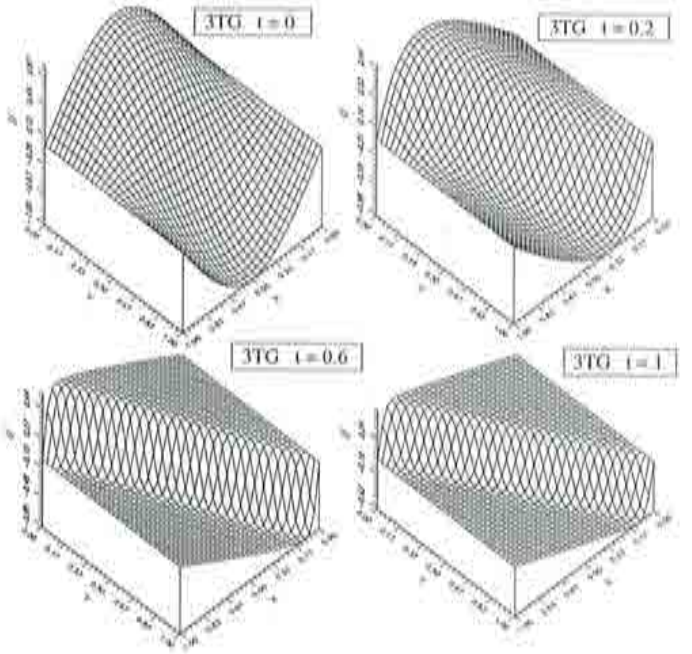

Figure 36: Solution $u(x, y, t)$ of 2D Burgers problem by $3TG$ with $Pe = 3.33$ for $c = 0.29$, $d = 0.09$.

9 Conclusions

In the present study, a major objective has been to achieve a high accuracy in the time integration of transient advection-diffusion problems.
Standard one-step Taylor-Galerkin (TG) methods are not ideally suited to deal with problems in this class, as their temporal accuracy is limited to second order if C^0 finite elements are employed for space discretization. This is in contrast with the pure advection case for which explicit and implicit Taylor-Galerkin schemes of higher order can be developed in connection with the use of C^0 finite elements.
In the first part of this report (Section 3), variants of the standard second-order accurate Taylor-Galerkin method have been introduced in the form of modified explicit TG methods. Such methods possess an extended stability domain with respect to the Lax-Wendroff finite element scheme $R_{2,0}$ though maintaining good phase and damping properties. They are, however, still limited to an overall second-order temporal accuracy.
To improve on this situation, we have shown in Section 4 how a multi-stage approach to Padé approximations of the exponential function can provide interesting explicit and implicit time-stepping methods of higher-order. Such methods only involve first time derivatives and are therefore easier to implement than Taylor-Galerkin methods in application to advection-diffusion problems.
Multi-stage explicit schemes of order three and four were derived which possess both higher accuracy and an extended stability domain with respect to second-order methods of the Lax-Wendroff or Taylor-Galerkin type.
In the area of implicit methods, Padé approximations of order three to six were presented and their practical implementation in the form of coupled equations involving first time derivatives only was discussed.
The properties of the multi-stage schemes derived from Padé approximations were studied in Section 5 as regards their domain of numerical stability and their phase and damping responses. It was shown that some implicit Padé schemes do possess remarquable accuracy properties while being unconditionally stable. Such schemes are therefore promising for achieving time-accurate solutions to transient advection-diffusion problems.
As regards the computer implementation of the implicit Padé methods $R_{2,2}$ and $R_{3,3}$, we have seen that the schemes obtained from Simpson/Lobatto quadrature (Section 7) are more compact than those obtained through the direct factorization of Padé approximations.
Runge-Kutta methods were considered in Section 6, as being methods involving first time derivatives only and possessing interesting stability properties. Actually, it appears that Runge-Kutta methods and multi-stage schemes derived from Padé approximations to the exponential function are intimely related and possess similar stability domains and phase and damping properties.
Numerical tests, including an original 2D Burgers problem with analytical so-

lution, have been performed to assess the performance of selected high-order Padé approximations in linear advection-diffusion problems. These first results have clearly shown that, when compared to traditional second-order methods, the high-order schemes permit the use of larger time-step values for an identical global time accuracy.
Implicit methods of high order appear competitive with respect to explicit methods in situations where the solution exhibits localized behaviour, thus requiring mesh refinement to achieve accurate results.
Further research efforts should be devoted to ways of improving the spatial accuracy and thereby achieve a uniformly high-order accurate computational method for transient advection-diffusion problems.

Acknowledgements
The present study has been performed during a scientific visit of the first author to the Departament de Matemàtica Aplicada III of the Universitat Politècnica de Catalunya. The support of the Spanish Ministerio de Educación y Ciencia, which made such visit possible, is gratefully acknowledged.

References

[1] J.H. Argyris, L.E. Vaz, K.J. Willam, 1977, Higher order methods for transient diffusion analysis, *Comput. Meths. Appl. Mech. Eng.*, **12**, 243–278.

[2] M. Crouzeix, 1979, Sur la B-stabilité de Méthodes Runge-Kutta, *Numerische Mathematik*, **32**, 75-82.

[3] J. Donea, 1984, A Taylor–Galerkin method for convective transport problems, *Int. J. Numer. Meths. Eng*, **20**, 101–120.

[4] J. Donea, S. Giuliani, H. Laval and L. Quartapelle, 1984, Time-accurate solution of advection–diffusion problems, *Comput. Meths. Appl. Mech. Eng*, **45**, 123–146.

[5] J. Donea, L. Quartapelle and V. Selmin, 1987, An analysis of time discretization in the finite element solution of hyperbolic problems, *J. Comput. Phys*, **70**, 463–499.

[6] J. Donea and L. Quartapelle, 1992, An introduction to finite element methods for transient advection problems, *Comput. Meths. Appl. Mech. Eng*, **95**, 169–203.

[7] J. Donea, V. Selmin and L. Quartapelle, 1989, Recent developments of the Taylor–Galerkin method for the numerical solution of hyperbolic problems, in *Numerical Methods for Fluid Dynamics III*, Eds. K. W. Morton and M. J. Baines, Clarendon Press, 171–185.

[8] C.W. GEAR, 1971, Numerical initial value problems in ordinary differential equations, *Prentice-Hall, Inc.*

[9] E. HAIRER, S.P. NØRSETT AND G. WANNER, 1987, Solving ordinary differential equations I, Nonstiff Problems, *Springer Series in Computational Mathematics.*

[10] E. HAIRER AND G. WANNER, 1991, Solving ordinary differential equations II, Stiff and Differential-algebraic Problems, *Springer Series in Computational Mathematics.*

[11] A. HARTEN AND H. TAL-EZER, 1981, On fourth order accurate implicit finite difference scheme for hyperbolic conservation laws: I. Nonstiff strongly dynamic problems, *Math. Comput.*, **36**, 335-373.

[12] D.M. HAWKEN, H.R. TAMADDON-JAHROMI, P. TOWNSEND AND M.F. WEBSTER, 1990, A Taylor-Galerkin based algorithm for viscous incompressible flow, *Int. J. Numer. Meths. Fluids*, **10**, 327-351.

[13] C. HIRSCH, 1990, Numerical computation of internal and external flows, *Computational methods for inviscid and viscous flows*, volume2, Wiley.

[14] T.J.R. HUGHES AND A. BROOKS, 1979, A multi-dimensional upwind scheme with no crosswind diffusion, *Finite Element Methods for Convection Dominated Flows*, T.J.R. Hughes (ed.) ASME, New York.

[15] C.B. JIANG AND M. KAWAHARA, 1993, The analysis of unsteady incompressible flows by a three-step finite element method, *Int. J. Numer. Meths. Fluids* , **21**, 885-900.

[16] K. KASHIYAMA, H. ITO, M. BEHR AND T. TEZDUYAR, 1995, Three-step explicit finite element computation of shallow water flows on a massively parallel computer, *Int. J. Numer. Meths. Fluids*, **21**, 885-900.

[17] J.D. LAMBERT, 1993, Numerical methods for ordinary differential systems, *John Wiley & Sons.*

[18] H. LAVAL AND L. QUARTAPELLE, 1990, A fractional-step Taylor–Galerkin method for unsteady incompressible flows, *Int. J. Numer. Meths. Fluids*, **11**, 501–513.

[19] J. PERAIRE, 1986, A finite element method for convection dominated flows, *Ph.D. Thesis, Univ. College of Swansea.*

[20] J. PERAIRE, O.C. ZIENKIEWICZ AND K. MORGAN, 1986, Shallow water problems: a general explicit formulation, *Int. J. Num. Meths. Eng.*, **22**, 547-574.

[21] A. Ralston and Ph. Rabinowitz, 1978, A First Course in Numerical Analysis, *McGraw-Hill*.

[22] R.D. Richtmyer and K.W. Morton, 1967, Difference Methods for Initial Value Problems, *Wiley Interscience*.

[23] P. Rogiest, 1997 An implicit finite volume scheme for the computation of unsteady compressible flows on multi-block structured grids. Application to aeroelastic problems. *Ph.D thesis*, University of Liège, Belgium.

[24] A. Sefjan and J. T. Oden, 1993, High-order Taylor–Galerkin and adaptive *hp*-methods for second order hyperbolic systems: Application to elastodynamics, *Comput. Meths. Appl. Mech. Eng*, **103**, 187-230.

[25] V. Selmin, 1986, Simulation par une méthode d'éléments finis de problèmes hyperboliques avec discontinuités', *Ph.D. Thesis*, Université de Liège.

[26] V. Selmin, J. Donea and L. Quartapelle, 1985, Finite element methods for nonlinear advection, *Comput. Meths. Appl. Mech. Eng*, **52**, 817–845.

[27] G. Staquet, 1996, Calcul d'écoulements compressibles instationnaires par une méthode implicite de volumes finis en maillages structurés, *Ph.D. Thesis*, Université de Liège.

[28] H.R. Tamaddon-Jahromi, D. Ding, M.F. Webster and P. Townsend, 1992, A Taylor-Galerkin finite element method for non-Newtonian flows, *Int. J. Numer. Meths. Eng*, **34**, 741-757.

[29] T.E. Tezduyar, S. Mittal and R. Shih, 1991, Time-accurate incompressible flow computations with quadrilateral velocity-pressure elements, *Comput. Meths. Appl. Mech. Eng*, **87**, 363–384.